PERGAMON

International Journal of Solids and Structures 40 (2003) 6217–6243

INTERNATIONAL JOURNAL OF SOLIDS and STRUCTURES

www.elsevier.com/locate/ijsolstr

Constitutive equations in finite viscoplasticity of semicrystalline polymers

A.D. Drozdov *, R.K. Gupta

Department of Chemical Engineering, West Virginia University, P.O. Box 6102, Morgantown, WV 26506, USA

Received 25 June 2003; received in revised form 25 June 2003

Abstract

Three series of uniaxial tensile tests with constant strain rates are performed at room temperature on isotactic polypropylene and two commercial grades of low-density polyethylene with different molecular weights. Constitutive equations are derived for the viscoplastic behavior of semicrystalline polymers at finite strains. A polymer is treated as an equivalent network of strands bridged by permanent junctions. Two types of junctions are introduced: affine whose micro-deformation coincides with the macro-deformation of a polymer, and non-affine that slide with respect to their reference positions. The elastic response of the network is attributed to elongation of strands, whereas its viscoplastic behavior is associated with sliding of junctions. The rate of sliding is proportional to the average stress in strands linked to non-affine junctions. Stress–strain relations in finite viscoplasticity of semicrystalline polymers are developed by using the laws of thermodynamics. The constitutive equations are applied to the analysis of uniaxial tension, uniaxial compression and simple shear of an incompressible medium. These relations involve three adjustable parameters that are found by fitting the experimental data. Fair agreement is demonstrated between the observations and the results of numerical simulation. It is revealed that the viscoplastic response of low-density polyethylene in simple shear is strongly affected by its molecular weight.

Keywords: Semicrystalline polymers; Low-density polyethylene; Isotactic polypropylene; Viscoplasticity; Finite strains

1. Introduction

This paper is concerned with the viscoplastic response of semicrystalline polymers at isothermal deformations with finite strains. The experimental part of the study focuses on the rate-dependent behavior of isotactic polypropylene (iPP) and two grades of low-density polyethylene (LDPE) with different molecular weights. The choice of iPP and LDPE for the investigation is explained by (i) their numerous industrial

* Corresponding author. Tel.: +1-304-293-2111; fax: +1-304-293-4139.
E-mail address: aleksey.drozdov@mail.wvu.edu (A.D. Drozdov).

0020-7683/$ - see front matter © 2003 Elsevier Ltd. All rights reserved.
doi:10.1016/S0020-7683(03)00414-1

applications (oriented films for packaging, reinforcing fibres, non-woven fabrics, pipes, wire coatings, fuel tanks, etc.), and (ii) variety of crystalline morphologies (ranging from monoclinic α spherulites in iPP to orthorhombic structures in LDPE) and molecular architectures in the amorphous phase of these polymers (ranging from short side branches to highly branched chains) that noticeably affect their mechanical and physical properties.

Isotactic polypropylene is a semicrystalline polymer containing three crystallographic forms: monoclinic α crystallites, hexagonal β structures, orthorhombic γ polymorphs, and "smectic" mesophase (Iijima and Strobl, 2000). At rapid cooling of the melt (at the stage of injection molding), α crystallites and smectic mesophase are mainly developed, whereas β and γ polymorphs are observed as minority components (Kalay and Bevis, 1997). A unique feature of the crystalline morphology of iPP is the lamellar cross-hatching: development of transverse lamellae oriented in the direction perpendicular to the direction of radial lamellae (Iijima and Strobl, 2000; Maiti et al., 2000). The characteristic size of spherulites in injection-molded specimens is estimated as 100–200 μm (Kalay and Bevis, 1997; Coulon et al., 1998). These spherulites consist of crystalline lamellae with thickness of 10–20 nm (Coulon et al., 1998; Maiti et al., 2000).

Low-density polyethylene is a semicrystalline polymer with orthorhombic crystalline structure. Linear chains in LDPE contain a large number of side branches (both short and long) that prevent macromolecules from packing closely in crystallites and result in a wide distribution of sizes of spherulites. The average radius of spherulites equals 3–12 μm (Graham et al., 1997). The spherulites are formed by lamellae stacks with lamellar thicknesses ranging from 8 to 12 nm (Matsuda et al., 2001). The average size of lamellae and their curvature, as well as the type of their organization into spherulites are strongly affected by crystallization conditions, molecular weight and the degree of branching of chains (Guichon et al., 2003).

The amorphous phase of iPP and LDPE is located (i) between spherulites, (ii) inside spherulites in "liquid pockets" between lamellar stacks (Verma et al., 1996), and (iii) between lamellae in lamellar stacks. It consists of (i) relatively mobile chains between spherulites and in liquid pockets, and (ii) severely restricted chains (the so-called rigid amorphous fraction: part of the amorphous phase whose molecular mobility is substantially suppressed by surrounding crystallites) (Verma et al., 1996).

In the past five years, viscoplasticity and yielding of iPP have been investigated by Coulon et al. (1998), Seguela et al. (1999) and Nitta and Takayanagi (1999, 2000). Viscoplasticity of polyethylene with relation to its crystalline morphology and topology of chains have been studied by Gaucher-Miri and Seguela (1997), Graham et al. (1997), Brooks et al. (1998, 1999a,b), Hiss et al. (1999), Hobeika et al. (2000) and Seguela (2002).

Deformation of a semicrystalline polymer at relatively small, but finite strains induces inter-lamellar separation, rotation and twist of lamellae, fine (homogeneous shear of layer-like crystalline structures) and coarse (heterogeneous inter-lamellar sliding) slip of lamellar blocks and their fragmentation (Gaucher-Miri and Seguela, 1997; Hiss et al., 1999), chain slip through the crystals, sliding and breakage of tie chains (Nitta and Takayanagi, 1999), detachment of chain folds and loops from the interfaces of crystal blocks (Gaucher-Miri and Seguela, 1997), and activation of the rigid amorphous fraction. At very large strains, disintegration of spherulites results in large-scale separation of lamellar blocks and transformation of spherulites into a fibrillar texture (Gaucher-Miri and Seguela, 1997; Nitta and Takayanagi, 2000), cavitation and stress-induced crystallization of chains in the amorphous phase.

To account for these morphological transformations in a constitutive model with a relatively small number of adjustable parameters, we apply a method of homogenization. According to it, a sophisticated micro-structure of a semicrystalline polymer is replaced by a single phase "whose internal micro-mechanical state is tracked as a function of applied deformation" (Bergström et al., 2002). As the equivalent phase, a network of macromolecules is conventionally chosen (Sweeney et al., 1997, 1999; Bergström et al., 2002) for the following reasons:

1. The time-dependent response of solid polymers is associated with rearrangement of chains in amorphous regions.
2. The viscoplastic flow in semicrystalline polymers is "initiated in the amorphous phase before transitioning into the crystalline phase" (Meyer and Pruitt, 2001).
3. Sliding of tie chains along and their detachment from lamellae play the key role in the yielding phenomenon (Nitta and Takayanagi, 1999).

To develop stress–strain relations in an explicit form, a network is treated as incompressible. Observations show that isotactic polypropylene and low-density polyethylene are weakly compressible polymers (Powers and Caddell, 1972). However, their compressibility is disregarded in the present study.

A semicrystalline polymer is modelled as a network of chains bridged by junctions (entanglements, physical cross-links on the surfaces of crystallites and lamellar blocks). All junctions are treated as permanent (chains cannot separate from their junctions during the experimental time scale), which implies that the viscoelastic effects associated with rearrangement of chains (Drozdov and Christiansen, 2002) are excluded from the consideration.

To describe the viscoplastic phenomena, the network is assumed to deform non-affinely: junctions can slide with respect to their reference positions under loading. Sliding of junctions in an equivalent network reflects (i) sliding of entanglements with respect to chains in the amorphous phase, (ii) slippage of tie chains along lamellar surfaces, and (iii) fine and coarse slip of crystalline lamellae. Unlike previous works in rheology of non-affine networks (Glatting et al., 1994; Wedgewood and Geurts, 1995; Sun et al., 2000), two types of junctions are introduced: affine (whose ability to slide is restricted by nearby chains in the amorphous phase and lamellar blocks), and non-affine (that can freely slide with respect to surrounding macromolecules). The novelty of the present approach compared to the previous study (Drozdov and Christiansen, 2003) is that we assume the rate-of-strain tensor for viscoplastic deformations to be proportional to the deviatoric component of the Cauchy stress tensor (not to the rate-of-strain tensor for macro-deformations). This allows a non-linear kinetic equation to be derived for the left Cauchy–Green tensor for elastic deformations similar to the differential equation for the evolution of the orientation tensor in the pom–pom model for branched polymer melts (Bishko et al., 1997; McLeish and Larson, 1998).

The objective of this work is threefold:

1. To report experimental data in uniaxial tensile tests with finite strains on isotactic polypropylene and two grades of low-density polyethylene with different molecular weights.
2. To develop constitutive equations for the viscoplastic behavior of a semicrystalline polymer and to determine adjustable parameters in the stress–strain relations by fitting the observations.
3. To demonstrate that the crystalline morphology and the molecular weight of semicrystalline polymers substantially affect their mechanical response.

The exposition is organized as follows. Experimental data in uniaxial tensile tests are reported in Section 2. Kinematic relations for non-affine deformation of an equivalent network are developed in Section 3. A kinetic equation for the rate-of-strain tensor for sliding of junctions is introduced in Section 4. Constitutive equations for a semicrystalline polymer at isothermal deformation with finite strains are derived in Section 5 by using the laws of thermodynamics. The stress–strain relations are simplified for uniaxial tension in Section 6 and for simple shear in Section 7. Adjustable parameters in the governing equations are determined in Section 8 by fitting observations in tensile tests. The dependencies of the material constants on the molecular weight and pressure are further investigated in Section 9 by matching experimental data in compression tests. Section 10 deals with numerical simulation of the viscoplastic behavior of LDPE in simple shear. Some concluding remarks are formulated in Section 11.

2. Experimental procedure

Isotactic polypropylene (Novolen 1100L) was supplied by BASF (Targor), low-density polyethylene (Lupolen 2410T) was donated by BASF (Basell), and low-density polyethylene (Huntsman PE 1020) was purchased from GE Plastics. Granules were dried at the temperature $T = 100$ °C for 12 h before molding in injection-molding machine Battenfeld 1000/315 CDC (Battenfeld). ASTM dumbbell specimens were injection-molded with length 148 mm, width 9.8 mm and thickness 3.8 mm.

The average molecular weights of two commercial grades of LDPE are not provided by the suppliers. Melt-flow index (MFI) of Lupolen 2410T equals 36 g/10 min (test method ISO 1133), whereas that of Huntsman PE 1020 equals 2 g/10 min (test method D 1238). As the melt-flow index is inversely proportional to $M^{3.4}$, where M is the weight-average molecular weight, Lupolen 2410T is treated as low-density polyethylene with low molecular weight, while Huntsman PE 1020 is referred to as low-density polyethylene with high molecular weight. For the sake of brevity, these polymers are abbreviated as LDPE-L and LDPE-H, respectively.

Uniaxial tensile tests were performed at room temperature on testing machines Instron-5568 (iPP and LDPE-L) and Instron-5869 (LDPE-H) equipped with electro-mechanical sensors for the control of longitudinal strains in the active zone of samples (with a distance of 50 mm between clips). The tensile force was measured by a standard load cell. The engineering stress σ_e was determined as the ratio of the axial force to the cross-sectional area of stress-free specimens.

Mechanical tests were carried out on samples not subjected to thermal pre-treatment. To minimize the effect of physical aging, experiments were performed at least three days after injection-molding. Each test was conducted on a new specimen. Necking of samples was not observed in experiments.

In the series of tests on LDPE-L, specimens were loaded with constant cross-head speeds of 5, 10, 25, 50, 100, 150 and 200 mm/min, which corresponded to the Hencky strain rates $\dot{\epsilon}_H = 9.80 \times 10^{-4}$, 2.03×10^{-3}, 5.16×10^{-3}, 9.92×10^{-3}, 2.07×10^{-2}, 3.03×10^{-2} and 4.00×10^{-2} s^{-1}, respectively, up to the maximal Hencky strain $\epsilon_{H\,max} = 0.3$.

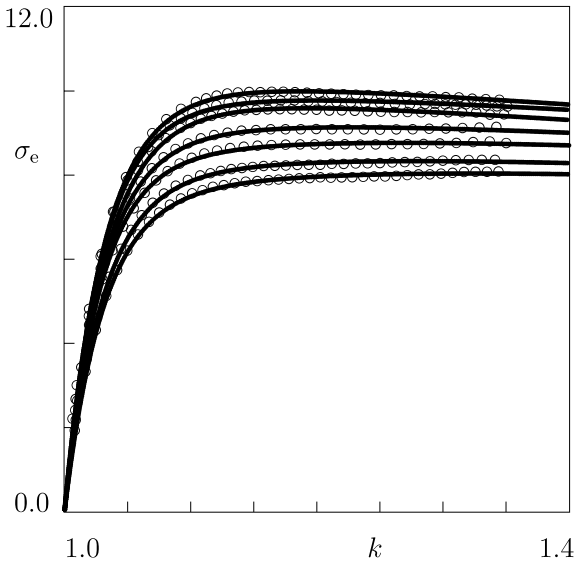

Fig. 1. The engineering stress σ_e MPa versus the elongation ratio k in tensile tests with the cross-head speeds 5, 10, 25, 50, 100, 150 and 200 mm/min from bottom to top, respectively. Circles: experimental data for LDPE-L. Solid lines: results of numerical simulation.

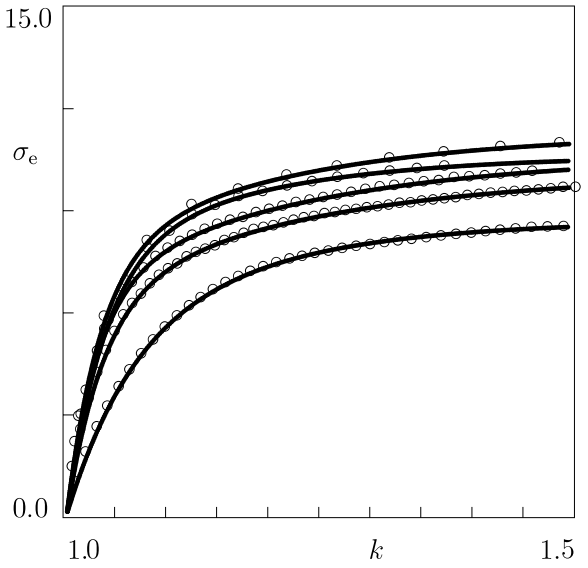

Fig. 2. The engineering stress σ_e MPa versus the elongation ratio k in tensile tests with the cross-head speeds 3, 13, 25, 127 and 254 mm/min. Circles: experimental data for LDPE-H. Solid lines: results of numerical simulation.

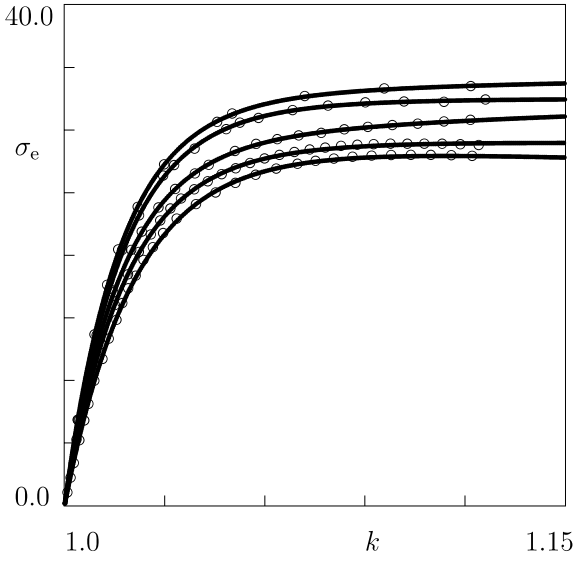

Fig. 3. The engineering stress σ_e MPa versus the elongation ratio k in tensile tests with the cross-head speeds 5, 10, 30, 50 and 100 mm/min from bottom to top, respectively. Circles: experimental data for iPP. Solid lines: results of numerical simulation.

In the series of tests on LDPE-H, specimens were loaded with constant cross-head speeds of 3, 13, 25, 127 and 254 mm/min (0.1, 0.5, 1.0, 5.0 and 10 in/min), which corresponded to $\dot{\epsilon}_H = 6.48 \times 10^{-4}$, 2.03×10^{-3}, 3.60×10^{-3}, 1.98×10^{-2} and 3.97×10^{-2} s^{-1}, respectively, up to the maximal Hencky strain $\epsilon_{H\,max} = 0.4$.

In the series of tests on iPP, specimens were loaded with constant cross-head speeds of 5, 10, 30, 50 and 100 mm/min, which corresponded to $\dot{\epsilon}_H = 9.80 \times 10^{-4}$, 2.03×10^{-3}, 7.16×10^{-3}, 9.92×10^{-3} and 2.07×10^{-2}, respectively, up to the maximal Hencky strain $\epsilon_{H\,max} = 0.12$. This relatively small value of the maximal strain was chosen to avoid necking of specimens at the cross-head speeds of 50 and 100 mm/min.

The chosen strain rates ensured nearly isothermal experimental conditions, on the one hand, and they allowed the viscoelastic effects to be disregarded, on the other.

The engineering stress σ_e is plotted versus the elongation ratio k in Figs. 1–3. The stress–strain diagrams show that (i) the dependence of stress σ_e on the engineering strain $\epsilon_e = k - 1$ is strongly non-linear even at relatively small strains, and (ii) given an elongation ratio k, the stress σ_e monotonically increases with the strain rate.

For LDPE-L, the engineering stress strongly increases with k in the initial region of deformations, reaches its ultimate value in the vicinity of the point $k \approx 1.15$, and weakly decreases afterwards. For LDPE-H, σ_e monotonically increases with k in the entire region of deformations under consideration. For iPP, the stress σ_e increases with k in the initial region of deformations and remains practically constant when k exceeds 1.09. It is worth noting that Figs. 1–3 present the dependence of the engineering stress σ_e on the elongation ratio k. The true stress estimated (based on the incompressibility condition) as $\sigma_t = \sigma_e k$ monotonically grows with k for all three polymers.

Our aim now is to develop constitutive equations that correctly describe the experimental data depicted in Figs. 1–3.

3. Kinematics of sliding

A semicrystalline polymer is treated as an incompressible permanent network of strands bridged by junctions (entanglements between chains in the amorphous regions, physical cross-links at the surfaces of crystallites and lamellar blocks). Macro-deformation of the network induces sliding (non-affine motion) of some part of the junctions with respect to their reference positions. In this section, kinematic relations are developed for the left and right Cauchy–Green tensors for elastic deformation of a non-affine network.

With reference to the conventional concepts in non-linear mechanics (Haupt, 2000), three configurations of an arbitrary element are introduced: (i) the reference configuration describes the position of this element before application of external loads, (ii) the actual configuration characterizes its position in the deformed state, and (iii) the intermediate configuration determines the current position of junctions driven by their sliding. Transformation of the reference state of a network into its actual state at time $t \geqslant 0$ is determined by the deformation gradient $\mathbf{F}(t)$. Transformation of the reference state into the intermediate state is characterized by the deformation gradient $\mathbf{F}_p(t)$, where the subscript index "p" indicates that non-affine motion of junctions is associated with their viscoplastic flow. Transformation of the intermediate state into the deformed state is described by the deformation gradient $\mathbf{F}_e(t)$, where the subscript index "e" means that $\mathbf{F}_e$ reflects elastic deformation of the network (in the sense that its mechanical energy is as a function of $\mathbf{F}_e$). The tensors $\mathbf{F}(t)$, $\mathbf{F}_e(t)$ and $\mathbf{F}_p(t)$ are connected by the multiplicative decomposition formula (Lee, 1969)

$$\mathbf{F}(t) = \mathbf{F}_e(t) \cdot \mathbf{F}_p(t), \tag{1}$$

where the dot stands for the standard dot product of tensors (Drozdov, 1998). Eq. (1) was proposed for non-affine networks in Buckley and Jones (1995), where $\mathbf{F}_e$ and $\mathbf{F}_p$ were identified as the "network stretch" tensor and the "slippage stretch" tensor.

The derivatives of the tensor $\mathbf{F}(t)$ and its inverse $\mathbf{F}^{-1}(t)$ with respect to time t read

$$\frac{d\mathbf{F}}{dt}(t) = \mathbf{L}(t) \cdot \mathbf{F}(t), \quad \frac{d\mathbf{F}^{-1}}{dt}(t) = -\mathbf{F}^{-1}(t) \cdot \mathbf{L}(t), \tag{2}$$

where $\mathbf{L}(t)$ is the velocity gradient in the actual state. The derivatives of the tensors $\mathbf{F}_p(t)$ and $\mathbf{F}_p^{-1}(t)$ are given by the formulas similar to Eqs. (2),

$$\frac{d\mathbf{F}_p}{dt}(t) = \mathbf{L}_p(t)\cdot\mathbf{F}_p(t), \quad \frac{d\mathbf{F}_p^{-1}}{dt}(t) = -\mathbf{F}_p^{-1}(t)\cdot\mathbf{L}_p(t), \tag{3}$$

where $\mathbf{L}_p(t)$ is the velocity gradient for sliding of junctions. It follows from Eq. (1) that

$$\frac{d\mathbf{F}_e}{dt}(t) = \frac{d}{dt}[\mathbf{F}(t)\cdot\mathbf{F}_p^{-1}(t)] = \frac{d\mathbf{F}}{dt}(t)\cdot\mathbf{F}_p^{-1}(t) + \mathbf{F}(t)\cdot\frac{d\mathbf{F}_p^{-1}}{dt}(t).$$

Substitution of Eqs. (2) and (3) into this equality results in

$$\frac{d\mathbf{F}_e}{dt}(t) = \mathbf{L}(t)\cdot\mathbf{F}_e(t) - \mathbf{F}_e(t)\cdot\mathbf{L}_p(t). \tag{4}$$

The left and right Cauchy–Green tensors for elastic deformation are given by

$$\mathbf{B}_e(t) = \mathbf{F}_e(t)\cdot\mathbf{F}_e^T(t), \quad \mathbf{C}_e(t) = \mathbf{F}_e^T(t)\cdot\mathbf{F}_e(t), \tag{5}$$

where T stands for transpose. We differentiate the first equality in Eqs. (5) with respect to time, use Eq. (4) and find that

$$\frac{d\mathbf{B}_e}{dt}(t) = \mathbf{L}(t)\cdot\mathbf{B}_e(t) + \mathbf{B}_e(t)\cdot\mathbf{L}^T(t) - 2\mathbf{F}_e(t)\cdot\mathbf{D}_p(t)\cdot\mathbf{F}_e^T(t), \tag{6}$$

where

$$\mathbf{D}_p(t) = \frac{1}{2}[\mathbf{L}_p(t) + \mathbf{L}_p^T(t)]$$

is the rate-of-strain tensor for sliding of junctions. Similarly, differentiation of the other equality in Eqs. (5) implies that

$$\frac{d\mathbf{C}_e}{dt}(t) = 2\mathbf{F}_e^T(t)\cdot\mathbf{D}(t)\cdot\mathbf{F}_e(t) - \mathbf{L}_p^T(t)\cdot\mathbf{C}_e(t) - \mathbf{C}_e(t)\cdot\mathbf{L}_p(t), \tag{7}$$

where

$$\mathbf{D}(t) = \frac{1}{2}[\mathbf{L}(t) + \mathbf{L}^T(t)]$$

is the rate-of-strain tensor for macro-deformation. Bearing in mind that for any smooth tensor function $\mathbf{W}(t)$,

$$\frac{d\mathbf{W}^{-1}}{dt}(t) = -\mathbf{W}^{-1}(t)\cdot\frac{d\mathbf{W}}{dt}(t)\cdot\mathbf{W}^{-1}(t),$$

we find from Eq. (7) that

$$\frac{d\mathbf{C}_e^{-1}}{dt}(t) = -2\mathbf{F}_e^{-1}(t)\cdot\mathbf{D}(t)\cdot[\mathbf{F}_e^{-1}(t)]^T + \mathbf{C}_e^{-1}(t)\cdot\mathbf{L}_p^T(t) + \mathbf{L}_p(t)\cdot\mathbf{C}_e^{-1}(t). \tag{8}$$

The first principal invariant of the right Cauchy–Green tensor $\mathbf{C}_e(t)$ reads

$$J_{e1}(t) = \mathscr{I}_1(\mathbf{C}_e(t)) = \mathbf{C}_e(t) : \mathbf{I},$$

where $\mathscr{I}_1$ denotes the first invariant of a tensor, $\mathbf{I}$ is the unit tensor and the colon stands for convolution. Differentiating this equality with respect to time and using Eqs. (5) and (7), we obtain

$$\frac{\mathrm{d}J_{\mathrm{e}1}}{\mathrm{d}t}(t) = 2[\mathbf{B}_{\mathrm{e}}(t) : \mathbf{D}(t) - \mathbf{C}_{\mathrm{e}}(t) : \mathbf{D}_{\mathrm{p}}(t)]. \tag{9}$$

For an incompressible medium, the second principal invariant of the right Cauchy–Green tensor $\mathbf{C}_{\mathrm{e}}(t)$ is given by

$$J_{\mathrm{e}2}(t) = \mathscr{I}_1(\mathbf{C}_{\mathrm{e}}^{-1}(t)) = \mathbf{C}_{\mathrm{e}}^{-1}(t) : \mathbf{I}.$$

It follows from this equality and Eqs. (5) and (8) that

$$\frac{\mathrm{d}J_{\mathrm{e}2}}{\mathrm{d}t}(t) = -2[\mathbf{B}_{\mathrm{e}}^{-1}(t) : \mathbf{D}(t) - \mathbf{C}_{\mathrm{e}}^{-1}(t) : \mathbf{D}_{\mathrm{p}}(t)]. \tag{10}$$

Eqs. (9) and (10) imply that the derivative of an arbitrary smooth function $\Phi(J_{\mathrm{e}1}, J_{\mathrm{e}2})$ of the first two principal invariants of the right Cauchy–Green tensor for elastic deformation $\mathbf{C}_{\mathrm{e}}(t)$ with respect to time t is determined as

$$\frac{\mathrm{d}\Phi}{\mathrm{d}t}(J_{\mathrm{e}1}(t), J_{\mathrm{e}2}(t)) = 2\{[\Phi_1(t)\mathbf{B}_{\mathrm{e}}(t) - \Phi_2(t)\mathbf{B}_{\mathrm{e}}^{-1}(t)] : \mathbf{D}(t) - [\Phi_1(t)\mathbf{C}_{\mathrm{e}}(t) - \Phi_2(t)\mathbf{C}_{\mathrm{e}}^{-1}(t)] : \mathbf{D}_{\mathrm{p}}(t)\}, \tag{11}$$

where

$$\Phi_m(t) = \frac{\partial \Phi}{\partial J_{\mathrm{e}m}}(J_{\mathrm{e}1}(t), J_{\mathrm{e}2}(t)) \quad (m = 1, 2). \tag{12}$$

By analogy with Eqs. (5), we introduce the left and right Cauchy–Green tensors for transition from the reference state to the deformed state at time $t \geqslant 0$,

$$\mathbf{B}(t) = \mathbf{F}(t) \cdot \mathbf{F}^{\mathrm{T}}(t), \quad \mathbf{C}(t) = \mathbf{F}^{\mathrm{T}}(t) \cdot \mathbf{F}(t). \tag{13}$$

For an incompressible medium, the first two principal invariants of these tensors read

$$J_1(t) = \mathscr{I}_1(\mathbf{C}(t)) = \mathbf{C}(t) : \mathbf{I}, \quad J_2(t) = \mathscr{I}_1(\mathbf{C}^{-1}(t)) = \mathbf{C}^{-1}(t) : \mathbf{I}.$$

The derivatives of the functions $J_1(t)$ and $J_2(t)$ with respect to time are determined by Eqs. (9) and (10), where the rate-of-stress tensor $\mathbf{D}_{\mathrm{p}}$ is omitted and the tensor $\mathbf{B}_{\mathrm{e}}$ is replaced by $\mathbf{B}$,

$$\frac{\mathrm{d}J_1}{\mathrm{d}t}(t) = 2\mathbf{B}(t) : \mathbf{D}(t), \quad \frac{\mathrm{d}J_2}{\mathrm{d}t}(t) = -2\mathbf{B}_{\mathrm{e}}^{-1}(t) : \mathbf{D}(t). \tag{14}$$

It follows from Eqs. (14) that the derivative of an arbitrary smooth function $\phi(J_1, J_2)$ of the first two principal invariants of the right Cauchy–Green tensor $\mathbf{C}(t)$ with respect to time t is given by

$$\frac{\mathrm{d}\phi}{\mathrm{d}t}(J_1(t), J_2(t)) = 2[\phi_1(t)\mathbf{B}(t) - \phi_2(t)\mathbf{B}^{-1}(t)] : \mathbf{D}(t), \tag{15}$$

where the functions $\phi_1(t)$ and $\phi_2(t)$ are determined by the formulas similar to Eqs. (12),

$$\phi_m(t) = \frac{\partial \phi}{\partial J_m}(J_1(t), J_2(t)) \quad (m = 1, 2). \tag{16}$$

Our aim now is to establish connections between the rate-of-strain tensor for sliding of junctions $\mathbf{D}_{\mathrm{p}}(t)$ and the Cauchy stress tensor for macro-deformation $\mathbf{\Sigma}(t)$.

4. Kinetics of sliding

According to the conventional approach in rational mechanics (Truesdell, 1977), the rate-of-strain tensor $\mathbf{D}_{\mathrm{p}}$ for viscoplastic deformation for an incompressible medium is an isotropic tensor function of the

deviatoric component $\boldsymbol{\Sigma}'$ of the stress tensor $\boldsymbol{\Sigma}$. Confining ourselves to linear relationships between the two tensors, we write

$$\mathbf{D}_{\mathrm{p}}(t) = a(t)\boldsymbol{\Sigma}'(t), \tag{17}$$

where a is a scalar material function. A substantial shortcoming of Eq. (17) is that it does not satisfy the objectivity condition (Haupt, 2000). To prove this assertion, we superpose rigid rotation in the actual state,

$$\mathbf{r}^0(t) = \mathbf{O}(t) \cdot \mathbf{r}(t), \tag{18}$$

where $\mathbf{r}(t)$ is the radius vector of an arbitrary point in the deformed state at time t, $\mathbf{r}^0(t)$ is its radius vector in the transformed state, and $\mathbf{O}(t)$ is an orthogonal tensor. Under transformation (18), the objective tensor $\boldsymbol{\Sigma}'$ is replaced by the tensor

$$\boldsymbol{\Sigma}^{0\prime}(t) = \mathbf{O}(t) \cdot \boldsymbol{\Sigma}'(t) \cdot \mathbf{O}^{\mathrm{T}}(t), \tag{19}$$

whereas the tensor $\mathbf{D}_{\mathrm{p}}(t)$ remains unchanged, because this tensor is uniquely determined by the radius vector in the intermediate configuration, which is not affected by rigid rotations in the deformed state.

To develop an analog of Eq. (17) that satisfies the objectivity condition, we introduce the left polar decomposition of the deformation gradient for transition from the intermediate state to the deformed state,

$$\mathbf{F}_{\mathrm{e}}(t) = \mathbf{V}_{\mathrm{e}}(t) \cdot \mathbf{R}_{\mathrm{e}}(t), \tag{20}$$

where $\mathbf{R}_{\mathrm{e}}(t)$ is an orthogonal rotation tensor, and $\mathbf{V}_{\mathrm{e}}(t)$ is a symmetric stretch tensor,

$$\mathbf{R}_{\mathrm{e}}^{\mathrm{T}}(t) = \mathbf{R}_{\mathrm{e}}^{-1}(t), \quad \mathbf{V}_{\mathrm{e}}^{\mathrm{T}}(t) = \mathbf{V}_{\mathrm{e}}(t).$$

Substitution of expression (20) into the first equality in Eqs. (5) implies that

$$\mathbf{V}_{\mathrm{e}}^2(t) = \mathbf{B}_{\mathrm{e}}(t). \tag{21}$$

Under rigid rotation in the deformed state, the elastic deformation gradient $\mathbf{F}_{\mathrm{e}}$ is replaced by the tensor

$$\mathbf{F}_{\mathrm{e}}^0(t) = \mathbf{O}(t) \cdot \mathbf{F}_{\mathrm{e}}(t). \tag{22}$$

It follows from Eqs. (5) and (22) that the left elastic Cauchy–Green tensor $\mathbf{B}_{\mathrm{e}}(t)$ is transformed as

$$\mathbf{B}_{\mathrm{e}}^0(t) = \mathbf{O}(t) \cdot \mathbf{B}_{\mathrm{e}}(t) \cdot \mathbf{O}^{\mathrm{T}}(t). \tag{23}$$

According to Eqs. (21) and (23), the elastic stretch tensor $\mathbf{V}_{\mathrm{e}}$ is replaced by the tensor

$$\mathbf{V}_{\mathrm{e}}^0(t) = \mathbf{O}(t) \cdot \mathbf{V}_{\mathrm{e}}(t) \cdot \mathbf{O}^{\mathrm{T}}(t). \tag{24}$$

Substitution of expressions (22) and (24) into Eq. (20) results in the formula for transformation of the rotation tensor,

$$\mathbf{R}_{\mathrm{e}}^0(t) = \mathbf{O}(t) \cdot \mathbf{R}_{\mathrm{e}}(t). \tag{25}$$

The deviatoric component of the Cauchy stress tensor $\boldsymbol{\Sigma}'$ is split into the sum of deviatoric components of two stress tensors,

$$\boldsymbol{\Sigma}'(t) = \boldsymbol{\Sigma}_{\mathrm{s}}'(t) + \boldsymbol{\Sigma}_{\mathrm{a}}'(t), \tag{26}$$

where $\boldsymbol{\Sigma}_{\mathrm{s}}'$ characterizes the extra stresses in strands linked to sliding junctions and $\boldsymbol{\Sigma}_{\mathrm{a}}'$ describes the extra stresses in strands with non-sliding (affine) junctions. The tensors $\boldsymbol{\Sigma}_{\mathrm{s}}'$ and $\boldsymbol{\Sigma}_{\mathrm{a}}'$ are assumed to transform according to the rule (19) under rigid rotation (18) in the actual state.

The following analog of Eq. (17) is introduced:

$$\mathbf{D}_{\mathrm{p}}(t) = a(t)\mathbf{R}_{\mathrm{e}}^{\mathrm{T}}(t) \cdot \boldsymbol{\Sigma}_{\mathrm{s}}'(t) \cdot \mathbf{R}_{\mathrm{e}}(t), \tag{27}$$

which implies that the rate of sliding of junctions is proportional to the stress arising due to stretching of chains linked to these junctions.

At small strains (when the tensor $\mathbf{R}_e$ may be replaced by the unit tensor $\mathbf{I}$), Eq. (27) coincides with kinetic equation (17), provided that all junctions are non-affine, $\mathbf{\Sigma}'_a = 0$. Substituting Eqs. (19) and (25) into Eq. (27), we find that this equation is objective (independent of rigid rotations in the deformed state). Finally, Eqs. (27) together with the orthogonality property of the rotation tensor $\mathbf{R}_e$ implies that for an incompressible network, the flow of junctions is volume preserving,

$$\mathscr{I}_1(\mathbf{D}_p(t)) = 0. \tag{28}$$

It follows from Eqs. (6), (20) and (27) that

$$\frac{d\mathbf{B}_e}{dt}(t) = \mathbf{L}(t)\cdot\mathbf{B}_e(t) + \mathbf{B}_e(t)\cdot\mathbf{L}^T(t) - 2a(t)\mathbf{V}_e(t)\cdot\mathbf{\Sigma}'_s(t)\cdot\mathbf{V}_e(t). \tag{29}$$

Eqs. (5), (20), (21) and (27) imply that

$$\begin{aligned}\mathbf{C}_e(t):\mathbf{D}_p(t) &= \mathscr{I}_1(\mathbf{F}_e^T(t)\cdot\mathbf{F}_e(t)\cdot\mathbf{D}_p(t)) = a(t)\mathscr{I}_1(\mathbf{R}_e(t)\cdot\mathbf{F}_e^T(t)\cdot\mathbf{F}_e(t)\cdot\mathbf{R}_e^T(t)\cdot\mathbf{\Sigma}'_s(t))\\ &= a(t)\mathscr{I}_1(\mathbf{V}_e^2(t)\cdot\mathbf{\Sigma}'_s(t)) = a(t)\mathbf{B}_e(t):\mathbf{\Sigma}'_s(t).\end{aligned}$$

By analogy with this equality, we find that

$$\mathbf{C}_e^{-1}(t):\mathbf{D}_p(t) = a(t)\mathbf{B}_e^{-1}(t):\mathbf{\Sigma}'_s(t).$$

Substitution of these expressions into Eq. (11) results in

$$\frac{d\Phi}{dt}(J_{e1}(t),J_{e2}(t)) = 2[\Phi_1(t)\mathbf{B}_e(t) - \Phi_2(t)\mathbf{B}_e^{-1}(t)]:[\mathbf{D}(t) - a(t)\mathbf{\Sigma}'_s(t)].$$

Bearing in mind that for any symmetric tensors, $\mathbf{A}_1$ and $\mathbf{A}_2$ such that $\mathscr{I}_1(\mathbf{A}_2) = 0$, we have

$$\mathbf{A}_1:\mathbf{A}_2 = \mathbf{A}'_1:\mathbf{A}_2,$$

where the prime stands for the deviatoric component of a tensor, and using the incompressibility condition $\mathscr{I}_1(\mathbf{D}) = 0$, we arrive at the formula

$$\frac{d\Phi}{dt}(J_{e1}(t),J_{e2}(t)) = 2[\Phi_1(t)\mathbf{B}_e(t) - \Phi_2(t)\mathbf{B}_e^{-1}(t)]':[\mathbf{D}(t) - a(t)\mathbf{\Sigma}'_s(t)]. \tag{30}$$

Our aim now is to apply Eqs. (15) and (30) in order to derive constitutive equations for an equivalent network of chains by using the laws of thermodynamics.

5. Constitutive equations

Denote by n_a the average number of affine junctions per unit volume, and by n_s the average number of sliding (non-affine) junctions. The quantities n_a and n_s are assumed to be independent of mechanical factors.

A strand is modelled as an incompressible isotropic elastic medium with the strain energy w that depends of two first principal invariants of an appropriate right Cauchy–Green tensor. For a strand linked to affine junctions, the strain energy w is a function of the invariants J_1 and J_2 of the tensor $\mathbf{C}$, whereas for a strand connected to sliding junctions, w is a function of the invariants J_{e1} and J_{e2} of the tensor $\mathbf{C}_e$. Neglecting the energy of interaction between strands (this energy is taken into account by the incompressibility condition), we determine the strain energy density of a polymer (per unit volume) as the sum of the mechanical energies of strands,

$$W = n_a w(J_1,J_2) + n_s w(J_{e1},J_{e2}). \tag{31}$$

For isothermal deformation of an incompressible medium at a reference temperature T_0, the Clausius–Duhem inequality reads (Haupt, 2000)

$$Q(t) = -\frac{dW}{dt}(t) + \boldsymbol{\Sigma}'(t) : \mathbf{D}(t) \geqslant 0, \tag{32}$$

where Q is internal dissipation per unit volume, and the deviatoric component $\boldsymbol{\Sigma}'$ of the Cauchy stress tensor $\boldsymbol{\Sigma}$ is determined by Eq. (26). Substituting expression (31) into Eq. (32) and using Eqs. (15), (26) and (30), we arrive at the formula

$$\begin{aligned} Q(t) = {} & \{\boldsymbol{\Sigma}_s'(t) - 2n_s[w_{e1}(t)\mathbf{B}_e(t) - w_{e2}(t)\mathbf{B}_e^{-1}(t)]'\} : \mathbf{D}(t) + \{\boldsymbol{\Sigma}_a'(t) - 2n_a[w_1(t)\mathbf{B}(t) - w_2(t)\mathbf{B}^{-1}(t)]'\} \\ & : \mathbf{D}(t) + 2a(t)n_s\boldsymbol{\Sigma}_s'(t) : [w_{e1}(t)\mathbf{B}_e(t) - w_{e2}(t)\mathbf{B}_e^{-1}(t)]' \geqslant 0, \end{aligned} \tag{33}$$

where the functions $w_{e1}(t)$ and $w_{e2}(t)$ are given by Eq. (12), the functions $w_1(t)$ and $w_2(t)$ are determined by Eq. (16), and the prime denotes the deviatoric component of a tensor. Inequality (33) is satisfied for an arbitrary program of loading, provided that the expressions in braces vanish,

$$\boldsymbol{\Sigma}_s'(t) = 2n_s[w_{e1}(t)\mathbf{B}_e(t) - w_{e2}(t)\mathbf{B}_e^{-1}(t)]', \quad \boldsymbol{\Sigma}_a'(t) = 2n_a[w_1(t)\mathbf{B}(t) - w_2(t)\mathbf{B}^{-1}(t)]'. \tag{34}$$

According to Eqs. (33) and (34), the internal dissipation per unit volume reads

$$Q(t) = a(t)\boldsymbol{\Sigma}_s' : \boldsymbol{\Sigma}_s' \geqslant 0.$$

Eqs. (26) and (34) imply the stress–strain relation

$$\boldsymbol{\Sigma}(t) = -P(t)\mathbf{I} + 2n_a[w_1(t)\mathbf{B}(t) - w_2(t)\mathbf{B}^{-1}(t)] + 2n_s[w_{e1}(t)\mathbf{B}_e(t) - w_{e2}(t)\mathbf{B}_e^{-1}(t)], \tag{35}$$

where $P(t)$ is pressure. Eq. (35) determines the Cauchy stress tensor $\boldsymbol{\Sigma}$ in terms of the left Cauchy–Green tensors for macro-deformation $\mathbf{B}$ and elastic deformation $\mathbf{B}_e$. When the number of sliding junctions n_s vanishes, Eq. (35) coincides with the conventional Finger formula for an elastic medium.

It follows from Eqs. (29) and (34) that the left Cauchy–Green tensor for elastic deformation $\mathbf{B}_e$ obeys the equality

$$\frac{d\mathbf{B}_e}{dt}(t) = \mathbf{L}(t)\cdot\mathbf{B}_e(t) + \mathbf{B}_e(t)\cdot\mathbf{L}^T(t) - 4a(t)n_s\mathbf{V}_e(t)\cdot[w_{e1}(t)\mathbf{B}_e(t) - w_{e2}(t)\mathbf{B}_e^{-1}(t)]'\cdot\mathbf{V}_e(t).$$

Bearing in mind that $\mathbf{A}' = \mathbf{A} - \frac{1}{3}\mathscr{I}_1(\mathbf{A})\mathbf{I}$ for an arbitrary symmetric tensor $\mathbf{A}$, and taking into account that for an incompressible medium,

$$\mathscr{I}_1(\mathbf{B}_e(t)) = J_{e1}(t), \quad \mathscr{I}_1(\mathbf{B}_e^{-1}(t)) = J_{e2}(t),$$

we find that

$$\begin{aligned} \frac{d\mathbf{B}_e}{dt}(t) = {} & \mathbf{L}(t)\cdot\mathbf{B}_e(t) + \mathbf{B}_e(t)\cdot\mathbf{L}^T(t) - 4a(t)n_s\mathbf{V}_e(t)\cdot[w_{e1}(t)\mathbf{B}_e(t) - w_{e2}(t)\mathbf{B}_e^{-1}(t)]\cdot\mathbf{V}_e(t) \\ & + \frac{4}{3}a(t)n_s[w_{e1}(t)J_{e1}(t) - w_{e2}(t)J_{e2}(t)]\mathbf{V}_e^2(t). \end{aligned} \tag{36}$$

It follows from Eq. (21) that

$$\mathbf{V}_e(t)\cdot\mathbf{B}_e(t)\cdot\mathbf{V}_e(t) = \mathbf{B}_e^2(t), \quad \mathbf{V}_e(t)\cdot\mathbf{B}_e^{-1}(t)\cdot\mathbf{V}_e(t) = \mathbf{I}.$$

Substitution of these expressions and Eq. (21) into Eq. (36) implies the kinetic equation for the left Cauchy–Green tensor for elastic deformation $\mathbf{B}_e$,

$$\frac{\mathrm{d}\mathbf{B}_{\mathrm{e}}}{\mathrm{d}t}(t)=\mathbf{L}(t)\cdot\mathbf{B}_{\mathrm{e}}(t)+\mathbf{B}_{\mathrm{e}}(t)\cdot\mathbf{L}^{\mathrm{T}}(t)-4a(t)n_{\mathrm{s}}\left\{w_{\mathrm{e}1}(t)\mathbf{B}_{\mathrm{e}}^{2}(t)-\frac{1}{3}[w_{\mathrm{e}1}(t)J_{\mathrm{e}1}(t)-w_{\mathrm{e}2}(t)J_{\mathrm{e}2}(t)]\mathbf{B}_{\mathrm{e}}(t)-w_{\mathrm{e}2}(t)\mathbf{I}\right\}. \tag{37}$$

Bearing in mind the dimensions of the rate-of-strain tensor for plastic flow $\mathbf{D}_{\mathrm{p}}$ and the stress tensor $\mathbf{\Sigma}'_{\mathrm{s}}$ in Eq. (27), it is convenient to present the coefficient a in the form

$$a(t)=\frac{D_i(t)}{\Sigma_{\mathrm{eq}}}, \tag{38}$$

where

$$D_i(t)=\left[\frac{2}{3}\mathbf{D}(t):\mathbf{D}(t)\right]^{1/2} \tag{39}$$

is the intensity of macro-strain rate, and Σ_{eq} is an equivalent stress. Combining Eqs. (37) and (38), we obtain

$$\frac{\mathrm{d}\mathbf{B}_{\mathrm{e}}}{\mathrm{d}t}(t)=\mathbf{L}(t)\cdot\mathbf{B}_{\mathrm{e}}(t)+\mathbf{B}_{\mathrm{e}}(t)\cdot\mathbf{L}^{\mathrm{T}}(t)-4n_{\mathrm{s}}\frac{D_i(t)}{\Sigma_{\mathrm{eq}}}\left\{w_{\mathrm{e}1}(t)\mathbf{B}_{\mathrm{e}}^{2}(t)-\frac{1}{3}[w_{\mathrm{e}1}(t)J_{\mathrm{e}1}(t)-w_{\mathrm{e}2}(t)J_{\mathrm{e}2}(t)]\mathbf{B}_{\mathrm{e}}(t)-w_{\mathrm{e}2}(t)\mathbf{I}\right\}. \tag{40}$$

In what follows, we concentrate on the mechanical response of a network of flexible chains (Treloar, 1975) with the mechanical energy

$$w(J_1,J_2)=c(J_1-3), \tag{41}$$

where c is the average rigidity per strand. Substitution of expressions (12), (16) and (41) into Eq. (35) results in the stress–strain relation

$$\mathbf{\Sigma}(t)=-P(t)\mathbf{I}+2\mu[\mathbf{B}_{\mathrm{e}}(t)+\varphi\mathbf{B}(t)], \tag{42}$$

where $\mu=cn_{\mathrm{s}}$ is an analog of the elastic modulus, $\varphi=n_{\mathrm{a}}/n_{\mathrm{s}}$ is the concentration of affine junctions, and the same notation P is used for the unknown pressure. Combining Eqs. (40) and (41) and using Eqs. (12) and (16), we arrive at the non-linear differential equation for the evolution of the tensor $\mathbf{B}_{\mathrm{e}}$,

$$\frac{\mathrm{d}\mathbf{B}_{\mathrm{e}}}{\mathrm{d}t}(t)=\mathbf{L}(t)\cdot\mathbf{B}_{\mathrm{e}}(t)+\mathbf{B}_{\mathrm{e}}(t)\cdot\mathbf{L}^{\mathrm{T}}(t)-\frac{4\mu D_i(t)}{\Sigma_{\mathrm{eq}}}\left[\mathbf{B}_{\mathrm{e}}^{2}(t)-\frac{1}{3}J_{\mathrm{e}1}(t)\mathbf{B}_{\mathrm{e}}(t)\right]. \tag{43}$$

Formulas (42) and (43) provide constitutive equations for the analysis of experimental data in three-dimensional mechanical tests. For an arbitrary loading with a constant strain rate D_i, these equations involve three material constants, μ, φ and Σ_{eq}, to be found by matching observations.

Our aim now is to simplify these relations for uniaxial tension and simple shear of a specimen. We confine ourselves to active deformation programs, when the elongation ratio and the coefficient of shear monotonically increase with time.

6. Uniaxial tension

Points of a medium refer to Cartesian coordinates $\{X_i\}$ ($i=1, 2, 3$) in the stress-free state, to Cartesian coordinates $\{x_i\}$ in the deformed state, and to Cartesian coordinates $\{\xi_i\}$ in the intermediate state at time $t\geqslant 0$. Uniaxial tension of the incompressible medium is described by the formulas

$$x_1=k(t)X_1,\quad x_2=k^{-1/2}(t)X_2,\quad x_3=k^{-1/2}(t)X_3, \tag{44}$$

where $k = k(t)$ is an elongation ratio. Transformation of the reference state into the intermediate state is determined by the equations similar to Eq. (44),

$$\xi_1 = \kappa(t)X_1, \quad \xi_2 = \kappa^{-1/2}(t)X_2, \quad \xi_3 = \kappa^{-1/2}(t)X_3, \tag{45}$$

where $\kappa(t)$ is a function to be found. It follows from Eqs. (44) and (45) that

$$\mathbf{B} = k^2\mathbf{e}_1\mathbf{e}_1 + \frac{1}{k}(\mathbf{e}_2\mathbf{e}_2 + \mathbf{e}_3\mathbf{e}_3), \quad \mathbf{B}_e = \left(\frac{k}{\kappa}\right)^2\mathbf{e}_1\mathbf{e}_1 + \frac{\kappa}{k}(\mathbf{e}_2\mathbf{e}_2 + \mathbf{e}_3\mathbf{e}_3), \tag{46}$$

where $\mathbf{e}_i$ are base vectors of the Cartesian frame $\{X_i\}$. According to Eq. (44), the velocity gradient $\mathbf{L}$ reads

$$\mathbf{L} = \frac{\dot{k}}{k}\left[\mathbf{e}_1\mathbf{e}_1 - \frac{1}{2}(\mathbf{e}_2\mathbf{e}_2 + \mathbf{e}_3\mathbf{e}_3)\right], \tag{47}$$

where $\dot{k}(t) = \mathrm{d}k(t)/\mathrm{d}t$. Eqs. (39) and (47) imply that

$$D_i = \frac{\dot{k}}{k}. \tag{48}$$

Substitution of expressions (46) into Eq. (42) results in

$$\mathbf{\Sigma} = \Sigma_1\mathbf{e}_1\mathbf{e}_1 + \Sigma_2(\mathbf{e}_2\mathbf{e}_2 + \mathbf{e}_3\mathbf{e}_3),$$

where the non-zero components of the Cauchy stress tensor are given by

$$\Sigma_1 = -P + 2\mu\left(\left(\frac{k}{\kappa}\right)^2 + \varphi k^2\right), \quad \Sigma_2 = -P + 2\mu\left(\frac{\kappa}{k} + \frac{\varphi}{k}\right).$$

Excluding the unknown pressure P from these equations and the boundary condition $\Sigma_2 = 0$ on the lateral surface of a specimen, we find the true longitudinal stress Σ_1,

$$\Sigma_1 = 2\mu\left[\left(\left(\frac{k}{\kappa}\right)^2 - \frac{\kappa}{k}\right) + \varphi\left(k^2 - \frac{1}{k}\right)\right].$$

The engineering tensile stress $\sigma_e = \Sigma_1/k$ reads

$$\sigma_e = \frac{2\mu}{k}\left[\left(\left(\frac{k}{\kappa}\right)^2 - \frac{\kappa}{k}\right) + \varphi\left(k^2 - \frac{1}{k}\right)\right]. \tag{49}$$

Substitution of expressions (46)–(48) into the kinetic equation (43) results in the differential equations

$$\frac{\mathrm{d}}{\mathrm{d}t}\left[\left(\frac{k}{\kappa}\right)^2\right] = \frac{2}{\kappa}\frac{\mathrm{d}k}{\mathrm{d}t}\left[\frac{k}{\kappa} - \frac{4\mu}{3\Sigma_{eq}}\left(\left(\frac{k}{\kappa}\right)^3 - 1\right)\right],$$

$$\frac{\mathrm{d}}{\mathrm{d}t}\left(\frac{\kappa}{k}\right) = -\frac{1}{\kappa}\frac{\mathrm{d}k}{\mathrm{d}t}\left[\left(\frac{\kappa}{k}\right)^2 - \frac{4\mu}{3\Sigma_{eq}}\left(1 - \left(\frac{\kappa}{k}\right)^3\right)\right].$$

These equations are equivalent to the only differential equation for the elongation ratio κ,

$$\frac{\mathrm{d}\kappa}{\mathrm{d}k} = \frac{4\mu}{3\Sigma_{eq}}\left[\frac{k}{\kappa} - \left(\frac{\kappa}{k}\right)^2\right], \quad \kappa(1) = 1. \tag{50}$$

Given a loading program $k = k(t)$, the tensile engineering stress σ_e is determined by Eq. (49), where the function κ obeys Eq. (50).

7. Simple shear

Simple shear of an incompressible medium is described by the formulas

$$x_1 = X_1 + kX_2, \quad x_2 = X_2, \quad x_3 = X_3, \tag{51}$$

where $k = k(t)$ is a coefficient of shear. Transformation of the reference state into the intermediate state is treated as a superposition of simple shear and three-dimensional extension,

$$\xi_1 = \lambda_1 X_1 + \kappa X_2, \quad \xi_2 = \lambda_2 X_2, \quad \xi_3 = \lambda_3 X_3, \tag{52}$$

where $\lambda_i = \lambda_i(t)$ and $\kappa = \kappa(t)$ are functions to be found. It follows from Eqs. (51) and (52) that the deformation gradients $\mathbf{F}$ and $\mathbf{F}_p$ are given by

$$\mathbf{F} = \begin{bmatrix} 1 & k & 0 \\ 0 & 1 & 0 \\ 0 & 0 & 1 \end{bmatrix}, \quad \mathbf{F}_p = \begin{bmatrix} \lambda_1 & \kappa & 0 \\ 0 & \lambda_2 & 0 \\ 0 & 0 & \lambda_3 \end{bmatrix}. \tag{53}$$

The incompressibility condition for the viscoplastic flow of junctions reads

$$\lambda_1 \lambda_2 \lambda_3 = 1. \tag{54}$$

Substituting expressions (53) into Eq. (1) and bearing in mind Eq. (54), we find that

$$\mathbf{F}_e = \begin{bmatrix} p_1 & \phi & 0 \\ 0 & p_2 & 0 \\ 0 & 0 & p_3 \end{bmatrix}, \tag{55}$$

where

$$p_1 = \lambda_2 \lambda_3, \quad p_2 = \lambda_1 \lambda_3, \quad p_3 = \lambda_1 \lambda_2, \quad \phi = \lambda_3(\lambda_1 k - \kappa), \quad \lambda_1 = p_1^{-1}, \quad \lambda_2 = p_2^{-1}, \quad \lambda_3 = p_3^{-1},$$
$$\kappa = p_1^{-1} k - p_3 \phi. \tag{56}$$

Eqs. (5), (13), (53) and (55) imply that

$$\mathbf{B} = \begin{bmatrix} 1 + k^2 & k & 0 \\ k & 1 & 0 \\ 0 & 0 & 1 \end{bmatrix}, \quad \mathbf{B}_e = \begin{bmatrix} \phi^2 + p_1^2 & \phi p_2 & 0 \\ \phi p_2 & p_2^2 & 0 \\ 0 & 0 & p_3^2 \end{bmatrix}. \tag{57}$$

According to Eq. (51), the velocity gradient $\mathbf{L}$ and the rate-of-strain tensor $\mathbf{D}$ are given by

$$\mathbf{L} = \dot{k} \begin{bmatrix} 0 & 1 & 0 \\ 0 & 0 & 0 \\ 0 & 0 & 0 \end{bmatrix}, \quad \mathbf{D} = \frac{\dot{k}}{2} \begin{bmatrix} 0 & 1 & 0 \\ 1 & 0 & 0 \\ 0 & 0 & 0 \end{bmatrix}. \tag{58}$$

It follows from Eqs. (39) and (58) that

$$D_i = \frac{\dot{k}}{\sqrt{3}}. \tag{59}$$

Substituting expressions (57)–(59) into Eq. (43), we arrive at the differential equations

$$\frac{d}{dt}(\phi^2 + p_1^2) = 2 \frac{dk}{dt} \left\{ \phi p_2 - \frac{2\mu}{\Sigma_{eq}\sqrt{3}} \left[(\phi^2 + p_1^2)^2 + \phi^2 p_2^2 - \frac{1}{3}(\phi^2 + p_1^2 + p_2^2 + p_3^2)(\phi^2 + p_1^2) \right] \right\},$$

$$\frac{d}{dt}(p_2^2) = -\frac{4\mu}{\Sigma_{eq}\sqrt{3}} \frac{dk}{dt} p_2^2 \left[(\phi^2 + p_2^2) - \frac{1}{3}(\phi^2 + p_1^2 + p_2^2 + p_3^2) \right],$$

$$\frac{\mathrm{d}}{\mathrm{d}t}(p_3^2) = -\frac{4\mu}{\Sigma_{\mathrm{eq}}\sqrt{3}}\frac{\mathrm{d}k}{\mathrm{d}t}p_3^2\left[p_3^2 - \frac{1}{3}(\phi^2 + p_1^2 + p_2^2 + p_3^2)\right],$$

$$\frac{\mathrm{d}}{\mathrm{d}t}(\phi p_2) = \frac{\mathrm{d}k}{\mathrm{d}t}\left\{p_2^2 - \frac{4\mu}{\Sigma_{\mathrm{eq}}\sqrt{3}}\phi p_2\left[(\phi^2 + p_1^2 + p_2^2) - \frac{1}{3}(\phi^2 + p_1^2 + p_2^2 + p_3^2)\right]\right\}.$$

Simple algebra implies that these equations may be presented in the form

$$\begin{aligned}
\frac{\mathrm{d}p_1}{\mathrm{d}k} &= -\frac{2\mu}{3\sqrt{3}\Sigma_{\mathrm{eq}}}p_1(2p_1^2 - p_2^2 - p_3^2 - \phi^2),\\
\frac{\mathrm{d}p_2}{\mathrm{d}k} &= -\frac{2\mu}{3\sqrt{3}\Sigma_{\mathrm{eq}}}p_2(-p_1^2 + 2p_2^2 - p_3^2 + 2\phi^2),\\
\frac{\mathrm{d}p_3}{\mathrm{d}k} &= -\frac{2\mu}{3\sqrt{3}\Sigma_{\mathrm{eq}}}p_3(-p_1^2 - p_2^2 + 2p_3^2 - \phi^2),
\end{aligned} \tag{60}$$

$$\frac{\mathrm{d}\phi}{\mathrm{d}k} = p_2 - \frac{2\mu}{3\sqrt{3}\Sigma_{\mathrm{eq}}}\phi(5p_1^2 + 2p_2^2 - p_3^2 + 2\phi^2). \tag{61}$$

The initial conditions for Eqs. (60) and (61) read

$$p_1(0) = 1, \quad p_2(0) = 1, \quad p_3(0) = 1, \quad \phi(0) = 0. \tag{62}$$

Multiplying the first equality in Eqs. (60) by p_2p_3, the other by p_1p_3, and the last by p_1p_2, and summing the obtained results, we find that

$$\frac{\mathrm{d}}{\mathrm{d}k}(p_1p_2p_3) = 0.$$

This formula together with Eqs. (56) and (62) implies that the incompressibility condition (54) is satisfied for an arbitrary shear k.

To determine components of the Cauchy stress tensor $\mathbf{\Sigma}$, we substitute expressions (57) into Eq. (42). We focus on the shear stress $\sigma = \Sigma_{12}$ and the first normal difference of stresses $N = \Sigma_{11} - \Sigma_{22}$, which are given by

$$\sigma = 2\mu(\phi p_2 + \varphi k), \quad N = 2\mu\left(\phi^2 + p_1^2 - p_2^2 + \varphi k^2\right). \tag{63}$$

Given a deformation program $k = k(t)$, the shear stress σ and the first normal difference N are determined by Eqs. (63), where the functions ϕ, p_1 and p_2 are governed by ordinary differential equations (60) and (61).

8. Fitting observations in tensile tests

In this section we find adjustable parameters μ, φ and Σ_{eq} in the constitutive equations by matching the experimental data in tensile tests depicted in Figs. 1–3 and analyze the effect of strain rate on the material constants.

We begin with fitting the observations on low-density polyethylene with low molecular weight presented in Fig. 1. Each stress–strain curve is approximated independently. To find the constants μ, φ and Σ_{eq} in Eqs. (49) and (50), we fix some intervals $[0, \varphi_{\max}]$ and $[0, C_{\max}]$, where the "best-fit" parameters φ and

$$C = \frac{4\mu}{3\Sigma_{\mathrm{eq}}} \tag{64}$$

are assumed to be located, and divide these intervals into J subintervals by the points $\varphi^{(i)} = i\Delta\mu$ and $C^{(j)} = j\Delta C$ $(i, j = 1, \ldots, J\text{–}1)$ with $\Delta\varphi = \varphi_{\max}/J$ and $\Delta C = C_{\max}/J$. For any pair $\{\varphi^{(i)}, C^{(j)}\}$, Eq. (50) is integrated numerically by the Runge–Kutta method with the step $\Delta k = 10^{-5}$. Given a pair $\{\varphi^{(i)}, C^{(j)}\}$, the elastic modulus μ is found by the least-squares method from the condition of minimum of the function

$$R = \sum_{k_n} \left[\sigma_{\exp}(k_n) - \sigma_{\text{num}}(k_n)\right]^2,$$

where the sum is calculated over all experimental points k_n depicted in Fig. 1, $\sigma_{\exp}$ is the engineering stress measured in a tensile test, and σ_{num} is given by Eq. (49). The "best-fit" parameters φ and C are determined from the condition of minimum of the function R on the set $\{\varphi^{(i)}, C^{(j)}\ (i, j = 1, \ldots, J\text{–}1)\}$. After finding the "best-fit" values $\varphi^{(i)}$ and $C^{(j)}$, this procedure is repeated twice for the new intervals $[\varphi^{(i-1)}, \varphi^{(i+1)}]$ and $[C^{(j-1)}, C^{(j+1)}]$, to ensure an acceptable accuracy of fitting. Given μ and C, the equivalent stress Σ_{eq} is found from Eq. (64).

The material constants μ, Σ_{eq} and φ that minimize the discrepancies between the experimental data and the results of numerical analysis are plotted versus the intensity of strain rate D_i in Figs. 4–6 (unfilled circles). The experimental data are approximated by the relations

$$\mu = \mu_0 + \mu_1 \log D_i, \quad \Sigma_{\text{eq}} = \Sigma_0 + \Sigma_1 \log D_i, \quad \varphi = \varphi_0 + \varphi_1 \log D_i, \tag{65}$$

where the adjustable parameters μ_m, Σ_m and φ_m $(m = 0, 1)$ are determined by the least-squares technique. The first two relations in Eqs. (65) are conventionally employed to describe the effect of strain rate on the elastic modulus and yield stress of solid polymers. It should be noted, however, that phenomenological equations (65) are fulfilled for a limited range of strain rates, and they cannot be extrapolated to very low strain rates.

Afterwards, the same procedure of fitting experimental data is repeated to approximate observations on low-density polyethylene with high molecular weight (Fig. 2) and isotactic polypropylene (Fig. 3). Figs. 1–3 demonstrate excellent agreement between the experimental data and the results of numerical simulation.

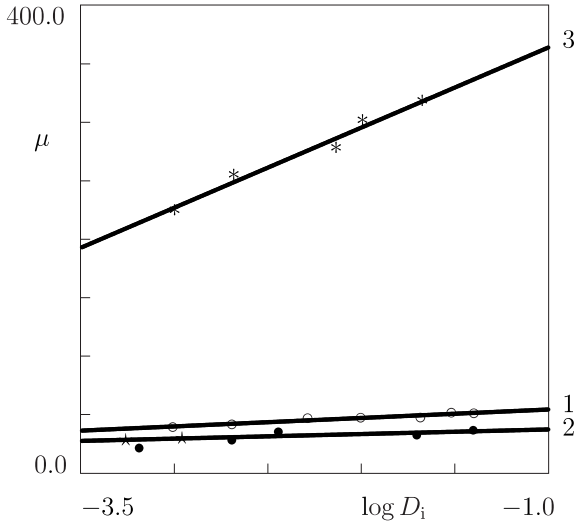

Fig. 4. The elastic modulus μ MPa versus the strain rate intensity D_i s^{-1}. Symbols: treatment of observations in tensile and compressive tests. Unfilled circles: LDPE-L. Filled circles: LDPE-H. Asterisks: iPP. Stars: LDPE-H in compressive tests. Solid lines: approximation of the experimental data by Eqs. (65). Curve 1: $\mu_0 = 61.45$, $\mu_1 = 7.23$. Curve 2: $\mu_0 = 41.08$, $\mu_1 = 3.92$. Curve 3: $\mu_0 = 432.57$, $\mu_1 = 68.53$.

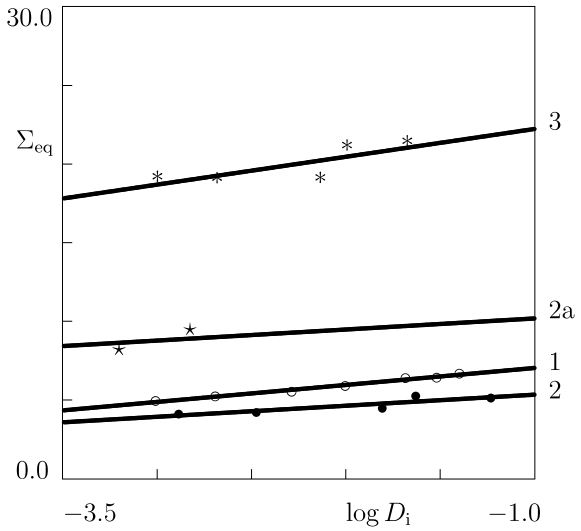

Fig. 5. The equivalent stress Σ_{eq} MPa versus the strain rate intensity D_i s^{-1}. Symbols: treatment of observations in tensile and compressive tests. Unfilled circles: LDPE-L. Filled circles: LDPE-H. Asterisks: iPP. Stars: LDPE-H in compressive tests. Solid lines: approximation of the experimental data by Eqs. (65). Curve 1: $\Sigma_0 = 8.11$, $\Sigma_1 = 1.08$. Curve 2: $\Sigma_0 = 6.65$, $\Sigma_1 = 0.88$. Curve 2a: $\Sigma_0 = 11.50$, $\Sigma_1 = 0.88$. Curve 3: $\Sigma_0 = 24.01$, $\Sigma_1 = 1.77$.

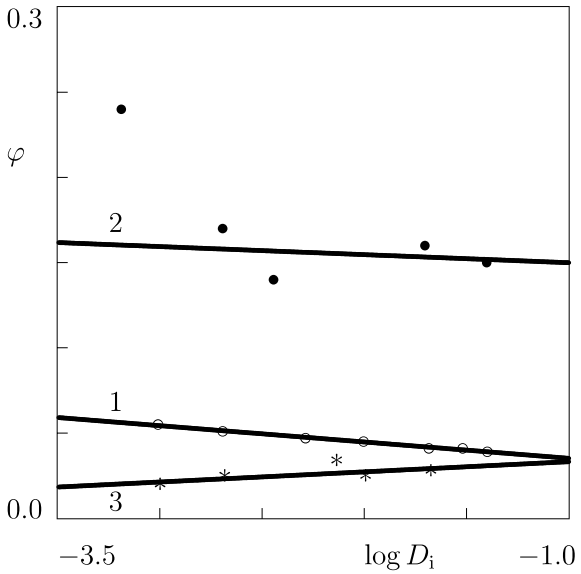

Fig. 6. The concentration of affine junctions φ versus the strain rate intensity D_i s^{-1}. Symbols: treatment of observations in tensile tests. Unfilled circles: LDPE-L. Filled circles: LDPE-H. Asterisks: iPP. Solid lines: approximation of the experimental data by Eqs. (65). Curve 1: $\varphi_0 = 2.56 \times 10^{-2}$, $\varphi_1 = -9.57 \times 10^{-3}$. Curve 2: $\varphi_0 = 1.45 \times 10^{-1}$, $\varphi_1 = -4.73 \times 10^{-3}$. Curve 3: $\varphi_0 = 3.91 \times 10^{-2}$, $\varphi_1 = 5.95 \times 10^{-3}$.

The adjustable parameters μ, Σ_{eq} and φ found by matching observations in tensile tests on LDPE-H and iPP are also depicted in Figs. 4–6 (filled circles and asterisks, respectively). These figures show that Eqs. (65)

correctly describe the effect of strain rate on the quantities μ, φ and Σ_{eq} (the only exception is the value of φ for LDPE-H at the smallest cross-head speed).

According to Fig. 4, the elastic modulus μ linearly grows with the logarithm of strain rate. The rate of increase is practically independent of chemical structure of the polymers under consideration: the ratio $r_\mu = \mu_1/\mu_0$ that characterizes this rate equals 0.12 for LDPE-L, 0.10 for LDPE-H and 0.16 for iPP. The modulus μ_0 is the largest for iPP and the smallest for LDPE-H.

To explain the dependence of the elastic modulus on strain rate, we recall that the model disregards viscoelasticity of semicrystalline polymers. According to the theory of transient networks (Tanaka and Edwards, 1992), the viscoelastic behavior of a network of chains reflects separation of active strands from temporary junctions and merging of dangling strands with the network. Detachment and attachment events occur at random times, when appropriate strands are excited by thermal fluctuations. To account (in a simple way) for rearrangement of a polymer network under deformation with a constant strain rate, we distinguish two groups of strands:

1. The characteristic time for rearrangement of strands belonging to the first group is substantially smaller than the characteristic time of macro-deformation (which means that stresses totally relax when these strands separate from their junctions, and the contribution of these strands into the strain energy density W is negligible).
2. The characteristic time for rearrangement of strands belonging to the other group noticeably exceeds the characteristic time for macro-deformation (which implies that detachment and attachment of these strands can be disregarded at the experimental time scale, and they may be treated as permanent).

According to this division of strands into two groups, the number (per unit volume) of strands bridged by permanent junctions monotonically grows with the strain rate, because an increase in the rate of macro-strain results in a decrease in the characteristic time of deformation, and, as a consequence, a decrease in the content of strands that rearrange under loading. Bearing in mind that the coefficient μ is proportional to the concentration of permanent strands, we conclude that the viscoelastic phenomena may be adequately described by assuming the elastic modulus to depend on strain rate in accord with phenomenological relation (65).

It is worth noting that the modulus μ is determined by fitting the entire stress–strain curves. This means that this modulus may substantially differ from the conventional Young modulus found by matching initial parts (corresponding to small strains) of the stress–strain diagrams. Comparison of our data with those reported by Lu and Sue (2002) shows that Young's moduli of LDPE-L and LDPE-H exceed appropriate values of μ by a factor of 3.

Fig. 4 demonstrates that the elastic modulus of LDPE with low molecular weight exceeds that of LDPE-H. At first glance, this conclusion seems paradoxical, because it contradicts the conventional standpoint in rubber elasticity, according to which elastic moduli increase with molecular weight (Treloar, 1975). This result may, however, be explained by the difference in the degrees of crystallinity of polyethylenes with different molecular weights. Graham et al. (1997) reported that the growth of the average molecular weight by twice (from 58,000 to 104,500 g/mol) implied a decrease in the degree of crystallinity by 25% (from 30% to 23%). As the elastic modulus of crystallites substantially exceeds that of the amorphous phase, a decrease in the degree of crystallinity induces in a pronounced reduction of moduli, in agreement with the observations depicted in Fig. 4.

Fig. 5 demonstrates that the equivalent stress Σ_{eq} linearly increases with the logarithm of strain rate following the same pattern as the elastic modulus μ. The slopes of the graphs depicted in Fig. 5 are weakly affected by chemical structure of the polymers: the ratio $r_\Sigma = \Sigma_1/\Sigma_0$ that characterizes these slopes equals 0.13 for LDPE-L and LDPE-H and 0.07 for iPP. It is worth noting a strong similarity between the values of r_μ and r_Σ, especially for the polyethylenes.

It is of interest to compare the equivalent stress Σ_{eq} with the yield stress Σ_y for these polymers (determined as the point of intersection between the tangent straight lines to the stress–strain diagrams at small and large strains, respectively). Comparison of Figs. 1–3 and 5 implies that for all three polymers, the ratio Σ_{eq}/Σ_y is constant and it equals approximately 0.6. Assuming Σ_{eq} to be proportional to the yield stress Σ_y, we conclude (based on the observations depicted in Fig. 5) that the yield stress of LDPE-L exceeds that of LDPE-H. This result is in agreement with the experimental data reported by Graham et al. (1997), which show that the growth of the molecular weight implies a decrease in the yield stress, and with observations by Brooks et al. (1999a), which reveal that the growth of the degree of crystallinity (Fig. 4 demonstrates that this parameter is higher for LDPE-L than for LDPE-H) causes an increase in the yield stress and a decrease in the yield strain.

According to Fig. 6, the ratio φ of the number of strands linked to affine junctions n_a to the number of strands connected to sliding junctions n_s decreases with strain rate for LDPE-L and LDPE-H and increases for iPP.

The reduction of φ with strain rate for polyethylenes seems quite natural. It means that the higher the strain rate D_i is, the more intensive is breakage of van der Waals links between strands (both in the amorphous and crystalline phase) that restrict molecular mobility of chains and prevent sliding of junctions. This implies that the number of strands connected to affine junctions n_a decreases with D_i, in accord with the observations depicted in Fig. 6.

Unlike the polyethylenes, the ratio φ for iPP increases with strain rate. The latter may be attributed to strain rate-induced fragmentation of transverse lamellae in spherulites, which results in release of the rigid amorphous phase, where mobility of junctions was severely restricted by lamellar cross-hatching. This implies that both parameters n_a and n_s grow with D_i, but an increase in n_a is more pronounced than that in n_s (after release of the rigid amorphous fraction, most junctions in the previously occluded domains move affinely), which is reflected by the growth of φ with strain rate.

One of the basic hypotheses in the theory of rubber elasticity (Treloar, 1975) is that junctions move affinely with the bulk material, which implies that sliding of junctions is thought of as an anomalous phenomenon. On the contrary, our analysis of experimental data in tensile tests (Fig. 6) reveals that sliding of junctions with respect to their reference positions is quite typical, whereas the concentration of affine (non-sliding) junctions is extremely small (a few percent for iPP and LDPE-L and less than 20% for LDPE-H).

Fig. 6 demonstrates that the value of φ for LDPE-H substantially exceeds that for LDPE-L (approximately by a factor of 5). This result may be explained as follows. As the elastic modulus of the crystalline phase substantially exceeds that of the amorphous phase, the viscoplastic response of a semicrystalline polymer (or, at least, its major part) may be associated with fine and coarse slip of lamellar blocks (Gaucher-Miri and Seguela, 1997; Seguela, 2002). This implies that affine motion of junctions (at which the deformation gradients for micro- and macro-deformations coincide) may be attributed to imperfectness of crystallites, because regular packing of chains in lamellae results in large friction between layer-like structures that causes a pronounced "delay" in their micro-deformation compared to the macro-deformation of a specimen. As a consequence, the content of affine junctions φ in LDPE-H noticeably exceeds that in LDPE-L, because the crystalline structures in LDPE with high molecular weight and highly branched chains are pronouncedly less perfect (and permit slip of crystalline layers at noticeably lower stresses) than those in LDPE with low molecular weight. The fact that the perfectness of crystallites in polyethylene is strongly affected by branching of chains and the concentration of entanglements was recently confirmed by differential scanning calorimetry (DSC) measurements (Fan et al., 2003).

To verify this explanation, we analyze the viscoplastic behavior of low-density polyethylene with high molecular weight (LDPE-H) in uniaxial compressive tests.

9. Uniaxial compression

As is well known (Drozdov, 1998), conventional constitutive models for rubber-like materials fail to correctly describe experimental data at compression when their material constants are determined by matching observations in uniaxial tensile tests with finite strains.

The purpose of this section is twofold: (i) to demonstrate that governing equations (49) and (50) adequately describe the stress–strain curves at compression, and (ii) to verify the following three conclusions drawn from the analysis of experimental data in tensile tests:

1. Derivation of Eq. (42) implies that the elastic modulus μ is independent of pressure P. Thus, it is natural to expect that the coefficient μ found by fitting experimental data at compression is close to that determined by matching observations at uniaxial tension.
2. According to conventional approaches in the plasticity theory for crystalline (Kuroda, 2003) and porous (Lee and Oung, 2000) materials, an increase in pressure results in the growth of the yield stress Σ_y of pressure-sensitive media. It is shown in Section 8 by fitting experimental data at uniaxial tension that the equivalent stress Σ_{eq} is proportional to Σ_y. As semicrystalline polymers are pressure-sensitive materials (Monasse et al., 1997; Butler et al., 1998; Brooks et al., 1999a), we expect that the equivalent stress at compression noticeably exceeds that at tension.
3. According to the hypothesis which associates affine junctions with lamellar blocks with negligible friction between layer-like structures, at compression, when hydrostatic pressure severely resists slippage of the layers with respect to one another, the concentration of affine junctions φ is essentially smaller than that under tension.

To validate these conclusions, two compressive tests were performed at room temperature on LDPE-H by using testing machine Instron-5869. The samples for the experimental analysis were injection-molded in the form of circular plates with diameter 61.8 mm and thickness 3.1 mm. Following protocol ASTM D-695, piles of 5 and 10 plates (the slenderness ratio of 1.0 and 2.0) were compressed with the relative rate of motion of grips 0.1 mm/min. For the piles, this speed corresponded to compressive Hencky strain rates $\dot{\epsilon}_H = 1.08 \times 10^{-3}$ and 5.38×10^{-4} s^{-1}, respectively. Before the tests, the specimens were slightly preloaded (the maximal compressive force at preloading was about 0.4 kN that corresponded to 1% of the maximal force in the experiments), to exclude fluctuations of stresses driven by possible warpage of plates and to ensure flatness of the surfaces of piles.

The maximal compressive Hencky strain was chosen to be $\epsilon_{H\,max} = 0.18$. Our choice is explained by the fact that the compressive load reaches 42 kN at this strain, whereas the maximal capacity of the load cell was 50 kN. The above value of the maximal compressive strain is close to $\epsilon_{max} = 0.13$ recommended by ASTM D-1621.

The compressive force was measured by a standard load cell. The deflection of specimens was determined from the cross-head movement. The engineering compressive stress σ_e was calculated as the ratio of the compressive force to the cross-sectional area of stress-free specimens.

Experiments were performed at least three days after injection-molding of samples. Each test was conducted on a new specimen.

The engineering compressive stress σ_e is plotted versus the compressive Hencky strain ϵ_H in Fig. 7. The stress–strain diagrams demonstrate strongly non-linear dependencies of stress σ_e on the strain ϵ_H and show that for a given Hencky strain ϵ_H, the stress σ_e monotonically increases with the strain rate.

For a uniaxial compression with a constant rate of Hencky strain $\dot{\epsilon}_H = -\dot{k}/k$, the kinetic equation (50) remains unchanged, whereas the stress–strain relation (49) for the engineering compressive stress reads

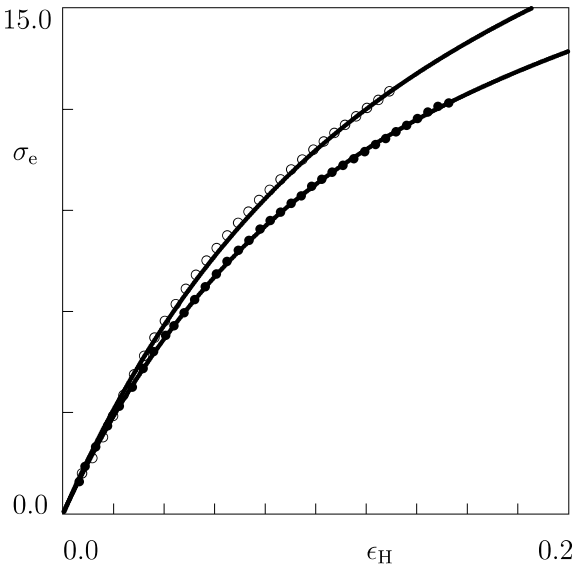

Fig. 7. The compressive engineering stress σ_e MPa versus the compressive Hencky strain ϵ_H in compressive tests with $\dot{\epsilon}_H = 1.08 \times 10^{-3}$ s^{-1} (unfilled circles) and $\dot{\epsilon}_H = 5.38 \times 10^{-4}$ s^{-1} (filled circles). Symbols: experimental data for LDPE-H. Solid lines: results of numerical simulation.

$$\sigma_e = -\frac{2\mu}{k}\left[\left(\left(\frac{k}{\kappa}\right)^2 - \frac{\kappa}{k}\right) + \varphi\left(k^2 - \frac{1}{k}\right)\right]. \tag{66}$$

The adjustable parameters μ, Σ_{eq} and φ in Eqs. (50) and (66) are determined by using the algorithm of matching observations described in Section 8. Fig. 7 demonstrates good correspondence between the experimental data and the results of numerical analysis.

The material constants μ, Σ_{eq} and φ that ensure the best-fit of observations are plotted versus the intensity of strain rate $D_i = \dot{\epsilon}_H$ in Figs. 4–6. According to Fig. 4, the values of the elastic modulus μ found by matching the stress–strain curves at compression (stars) are in excellent agreement with curve 2 that approximates the dependence of the elastic modulus on strain rate under tension.

Fig. 5 demonstrates that the equivalent stress Σ_{eq} at compression is higher (by twice) than that at tension, but it follows approximately the same dependence on strain rate (as we have only two experimental points at compression, the function $\Sigma_{eq}(D_i)$ is approximated by the straight line (65) with the same slope as that for uniaxial tension).

For both stress–strain curves depicted in Fig. 7, it is found that the "best-fit" value of φ equals zero. This means that application of hydrostatic pressure results in so pronounced increase in friction between layer-like structures in crystallites that affine junctions totally disappear.

These conclusions confirm the above hypotheses and demonstrate that the adjustable parameters of the model are affected by strain rate and pressure in a physically plausible way.

10. Numerical simulation of simple shear

In the approximation of the experimental data in tensile tests, a noticeable difference has been revealed between the values of φ for low-density polyethylenes with low and high molecular weights. The aim of this

section is to show that this quantitative difference implies a qualitative difference in the mechanical responses of LDPE-L and LDPE-H. For this purpose, we analyze numerically the effect of shear rate on the shear stress and the first normal difference of stresses at simple shear of an incompressible medium with finite strains.

Eqs. (60) and (61) with initial conditions (62) are integrated numerically by the Runge–Kutta method with the step $\Delta k = 10^{-4}$ in the interval between $k = 0$ and $k = 1$. Five shear rates $\dot{k} = 0.01$, 0.1, 1.0, 10.0 and 100.0 s^{-1} are employed in the numerical simulation. The shear stress σ and the first normal difference N are determined by Eqs. (63). The effect of strain rate on the adjustable parameters μ, Σ_{eq} and φ is described by Eqs. (65), where the strain rate intensity D_i is given by Eq. (59). We use the coefficients μ_m, Σ_m and φ_m ($m = 0$, 1) in Eqs. (65) found by fitting the experimental data for LDPE-L and LDPE-H depicted in Figs. 1 and 2. The shear stress σ and the first normal difference of stresses N are plotted versus the coefficient of shear k in Figs. 8 and 9 for LDPE-H and in Figs. 10 and 11 for LDPE-L, respectively.

Fig. 8 shows that at all strain rates under consideration, the shear stress σ rapidly increases with k in the initial interval of deformations ($k < 0.2$), and grows linearly with k afterwards. Given k, the shear stress monotonically increases with the strain rate, but this growth is rather modest: when the shear rate increases by four orders of magnitude, the shear stress grows by about 43%. Fig. 9 demonstrates that given a strain rate $\dot{k}$, the first normal difference of stresses N grows as a quadratic function of k. For a fixed k, the first normal difference weakly increases with the strain rate: by about 34% when $\dot{k}$ grows from 0.01 to 100 s^{-1}. After an initial period of deformations, when $k > 0.2$, the first normal difference of stresses N is proportional to the square of shear stress σ, in agreement with the Lodge–Meissner rule (Lodge and Meissner, 1972). According to Figs. 8 and 9, the rate-dependent response of LDPE with high molecular weight is quite typical of rubbery polymers and polymer melts.

Fig. 10 shows that given a shear rate $\dot{k}$, the shear stress σ monotonically increases with the coefficient of shear (rather strongly at the initial period of deformations, and linearly afterwards). Unlike LDPE-H, the slope of the curve $\sigma(k)$ for LDPE-L within the region of steady viscoplastic flow strongly depends on the strain rate and monotonically decreases with $\dot{k}$. This leads to intersection of the stress–strain curves at

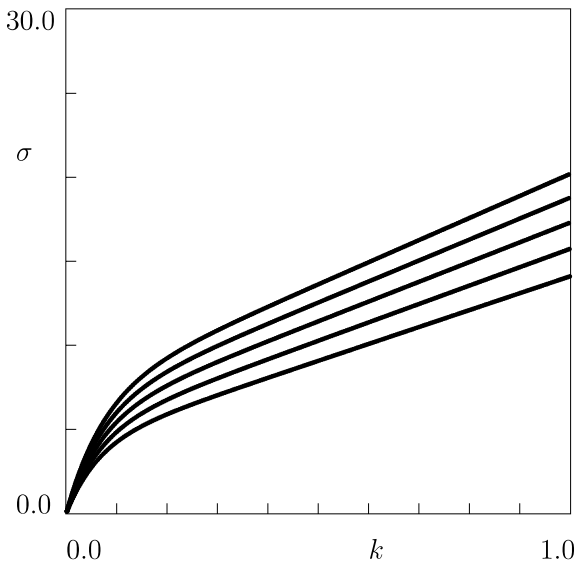

Fig. 8. The shear stress σ MPa versus the coefficient of shear k in shear tests with the strain rates $\dot{k} = 0.01$, 0.1, 1.0, 10.0 and 100.0 s^{-1} from bottom to top, respectively. Solid lines: results of numerical simulation for LDPE-H.

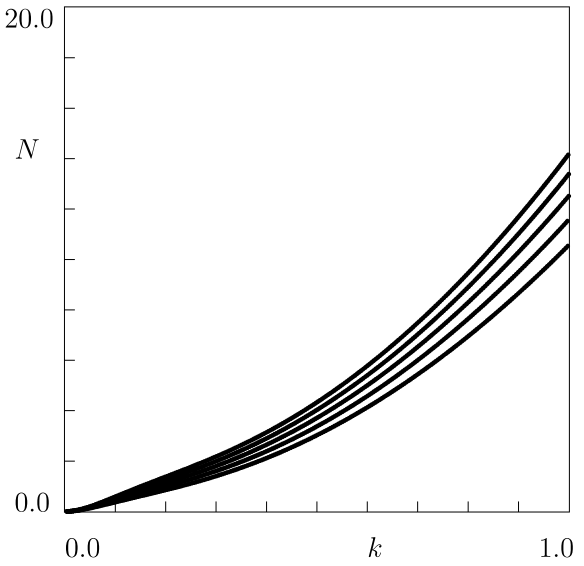

Fig. 9. The first normal difference N MPa versus the coefficient of shear k in shear tests with the strain rates $\dot{k} = 0.01$, 0.1, 1.0, 10.0 and 100.0 s^{-1} from bottom to top, respectively. Solid lines: results of numerical simulation for LDPE-H.

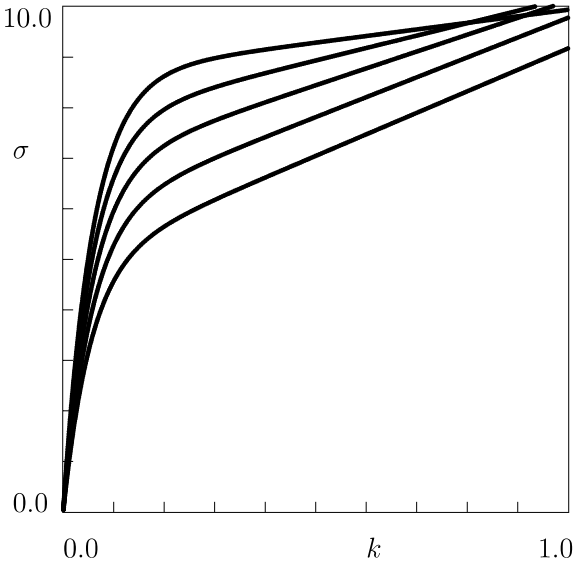

Fig. 10. The shear stress σ MPa versus the coefficient of shear k in shear tests with the strain rates $\dot{k} = 0.01$, 0.1, 1.0, 10.0 and 100.0 s^{-1} from bottom to top, respectively. Solid lines: results of numerical simulation for LDPE-L.

relatively large coefficients of shear. Fig. 11 demonstrates a rather sophisticated dependence of the first normal difference N on the coefficient of shear k. The function $N(k)$ reveals a pronounced shoulder near the point $k \approx 0.2$, which substantially grows with the shear rate. In the interval between $k = 0$ and $k = 0.4$, an increase in the shear rate results in the growth of the first normal difference of stresses. The stress–strain curves corresponding to different values of $\dot{k}$ intersect in the vicinity of the point $k = 0.4$, and at higher

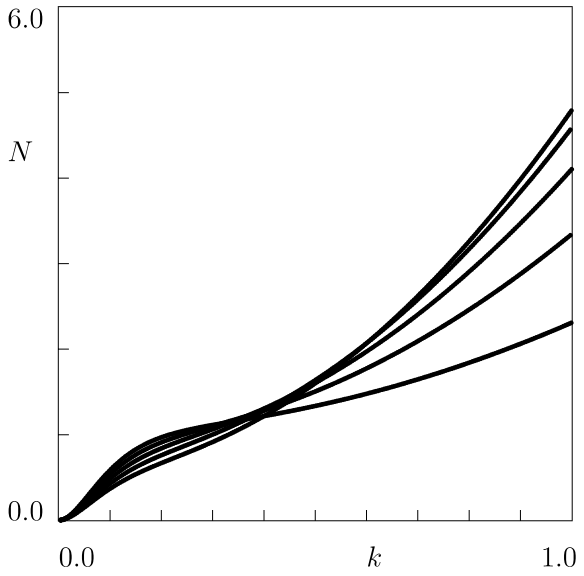

Fig. 11. The first normal difference N MPa versus the coefficient of shear k in shear tests with the strain rates $\dot{k} = 0.01$, 0.1, 1.0, 10.0 and 100.0 s^{-1} from bottom to top, respectively. Solid lines: results of numerical simulation for LDPE-L.

strains, an increase in the shear rate leads to a decrease in N. Although the Lodge–Meissner law is satisfied for a steady viscoplastic flow, the area of its applicability is noticeably shifted to relatively large strains.

The dependencies $\sigma(k)$ and $N(k)$ similar to those depicted in Figs. 10 and 11 have been previously observed in polymer solutions (Oberhauser et al., 1998; Osaki et al., 2000) and particle gels (Whittle and Dickinson, 1997). The results of numerical simulation demonstrate that semicrystalline polymers with relatively low molecular weight may also reveal such an "unusual" mechanical behavior at high shear rates.

11. Concluding remarks

Three series of tensile tests have been performed at ambient temperature on injection-molded isotactic polypropylene and two commercial grades of low-density polyethylene with low and high molecular weights. Experiments have been carried out at finite strains (up to 50%) with cross-head speeds ranging from 3 to 250 mm/min that cover the entire region of strain rates used in quasi-static tensile tests.

A constitutive model has been derived for the isothermal viscoplastic behavior of semicrystalline polymers at finite strains. A polymer is treated as an equivalent network of chains bridged by permanent junctions. Two types of junctions are introduced: (i) affine whose micro-deformation coincides with macro-deformation of a specimen, and (ii) sliding that slip with respect to their reference positions under loading. Sliding of junctions reflects (i) sliding of entanglements with respect to chains in the amorphous phase, (ii) slippage of tie chains along lamellar surfaces, and (iii) fine and coarse slip of lamellar blocks. The rate of sliding of junctions is proportional to the intensity of macro-stresses.

Constitutive equations for an equivalent non-affine network of chains are developed by using the laws of thermodynamics. The governing equations consist of stress–strain relation (35) and a non-linear differential equation (40) for the evolution of the left Cauchy–Green tensor for elastic deformation. For a Gaussian network of flexible chains, these relations involve three material parameters: the elastic modulus μ, the equivalent stress Σ_{eq} and the concentration of affine junctions φ.

The constitutive equations are simplified for uniaxial tension and simple shear of an incompressible medium with finite strains. The material constants are found by fitting the observations in tensile tests with various strain rates. Fair agreement is demonstrated between the experimental data and the results of numerical simulation.

The following conclusions are drawn:

1. The modulus μ is independent of pressure, and it monotonically increases with the intensity of strain rate D_i. This growth may be explained by the material viscoelasticity. The slopes of the graphs $\mu(D_i)$ are similar for the polyolefins under consideration. The modulus of LDPE with low molecular weight exceeds that of LDPE with high molecular weight, which is associated with a smaller degree of crystallinity in LDPE-H.
2. The equivalent stress Σ_{eq} increases with strain rate in the same way as the yield stress Σ_y determined by conventional methods. The rate of increase is the highest for polyethylenes (and it is independent of their molecular weight) and the lowest for polypropylene. The equivalent stress at compression noticeably exceeds that at tension.
3. The ratio φ decreases with strain rate for polyethylenes (due to the rate-induced breakage of links between chains which prevented sliding of junctions in a stress-free medium) and increases for iPP (which is attributed to fragmentation of tangential lamellae and release of the rigid amorphous fraction). The content of affine junctions in LDPE with high molecular weight noticeably exceeds that in LDPE with low molecular weight (this reflects the difference in the perfectness of crystals of the two grades of polyethylene). The concentration of affine junctions at tension is substantially higher than that at compression (because hydrostatic pressure increases friction between layer-like structures in crystallites and prevents their slippage with respect to one another).
4. The quantitative difference between the values of φ for LDPE-L and LDPE-H results in a qualitative difference in their responses at simple shear. The behavior of LDPE with high molecular weight is similar to that of elastomers and polymer melts (monotonic dependencies of the shear stress and the first normal difference of stresses on the coefficient of shear and the rate of shear). On the contrary, LDPE with low molecular weight reveals a pattern typical of polymer solutions and suspensions of particles (a non-monotonic dependence of the first normal difference on the coefficient of shear at high shear rates).

Acknowledgements

This work was partially supported by the US Department of Energy through grant DE–FC26–00FT40598 and by the West Virginia Research Challenge Grant Program.

References

Bergström, J.S., Kurtz, S.M., Rimnac, C.M., Edidin, A.A., 2002. Constitutive modeling of ultra-high molecular weight polyethylene under large-deformation and cyclic conditions. Biomaterials 23, 2329–2343.

Bishko, G., McLeish, T.C.B., Harlen, O.G., Larson, R.G., 1997. Theoretical molecular rheology of branched polymers in simple and complex flows: the pom–pom model. Physical Review Letters 79, 2352–2355.

Brooks, N.W.J., Duckett, R.A., Ward, I.M., 1998. Temperature and strain-rate dependence of yield stress of polyethylene. Journal of Polymer Science. Part B: Polymer Physics 36, 2177–2190.

Brooks, N.W.J., Duckett, R.A., Ward, I.M., 1999a. Effects of crystallinity and stress state on the yield strain of polyethylene. Polymer 40, 7367–7372.

Brooks, N.W., Ghazali, M., Duckett, R.A., Unwin, A.P., Ward, I.M., 1999b. Effects of morphology on the yield stress of polyethylene. Polymer 40, 821–825.

Buckley, C.P., Jones, D.C., 1995. Glass–rubber constitutive model for amorphous polymers near the glass transition. Polymer 36, 3301–3312.

Butler, M.F., Donald, A.M., Ryan, A.J., 1998. Time resolved simultaneous small- and wide-angle X-ray scattering during polyethylene deformation. 3. Compression of polyethylene. Polymer 39, 781–792.

Coulon, G., Castelein, G., G'Sell, C., 1998. Scanning force microscopic investigation of plasticity and damage mechanisms in polypropylene spherulites under simple shear. Polymer 40, 95–110.

Drozdov, A.D., 1998. Mechanics of Viscoelastic Solids. Wiley, Chichester.

Drozdov, A.D., Christiansen, J.deC., 2002. The effect of annealing on the time-dependent behavior of isotactic polypropylene at finite strains. Polymer 43, 4745–4761.

Drozdov, A.D., Christiansen, J.deC., 2003. The effect of annealing on the viscoplastic response of semicrystalline polymers at finite strains. International Journal of Solids and Structures 40, 1337–1367.

Fan, Z., Wang, Y., Bu, H., 2003. Influence of intermolecular entanglements on crystallization behavior of ultra-high molar mass polyethylene. Polymer Engineering and Science 43, 607–614.

Gaucher-Miri, V., Seguela, R., 1997. Tensile yield of polyethylene and related copolymers, mechanical and structural evidences of two thermally activated processes. Macromolecules 30, 1158–1167.

Glatting, G., Winkler, R.G., Reineker, P., 1994. Analytical model of the microscopic non-affine deformation of polymer networks. Journal of Chemical Physics 101, 2532–2538.

Graham, J.T., Alamo, R.G., Mandelkern, L., 1997. The effect of molecular weight and crystallite structure on yielding in ethylene copolymers. Journal of Polymer Science. Part B: Polymer Physics 35, 213–223.

Guichon, O., Seguela, R., David, L., Vigier, G., 2003. Influence of the molecular architecture of low-density polyethylene on the texture and mechanical properties of blown films. Journal of Polymer Science. Part B: Polymer Physics 41, 327–340.

Haupt, P., 2000. Continuum Mechanics and Theory of Materials. Springer, Berlin.

Hiss, R., Hobeika, S., Lynn, C., Strobl, G., 1999. Network stretching, slip processes, and fragmentation of crystallites during uniaxial drawing of polyethylene and related copolymers. A comparative study. Macromolecules 32, 4390–4403.

Hobeika, S., Men, Y., Strobl, G., 2000. Temperature and strain rate independence of critical strains in polyethylene and poly(ethylene-*co*-vinyl acetate). Macromolecules 33, 1827–1833.

Iijima, M., Strobl, G., 2000. Isothermal crystallization and melting of isotactic polypropylene analyzed by time- and temperature-dependent small-angle X-ray scattering experiments. Macromolecules 33, 5204–5214.

Kalay, G., Bevis, M.J., 1997. Processing and physical property relationships in injection-molded isotactic polypropylene. 2. Morphology and crystallinity. Journal of Polymer Science. Part B: Polymer Physics 35, 265–291.

Kuroda, M., 2003. Crystal plasticity model accounting for pressure dependence of yielding and plastic volume expansion. Scripta Materialia 48, 605–610.

Lee, E.H., 1969. Elastic-plastic deformation at finite strains. Journal of Applied Mechanics 36, 1–6.

Lee, J.H., Oung, J., 2000. Yield functions and flow rules for porous pressure-dependent strain-hardening polymeric materials. Journal of Applied Mechanics 67, 288–297.

Lodge, A.S., Meissner, J., 1972. On the use of instantaneous strains, superposed on shear and elongation flows of polymeric liquids, to test the Gaussian network hypothesis and to estimate the segment concentration and its variation during flow. Rheologica Acta 11, 351–352.

Lu, J., Sue, H.-J., 2002. Morphology and mechanical properties of blown films of a low-density polyethylene/linear low-density polyethylene blend. Journal of Polymer Science. Part B: Polymer Physics 40, 507–518.

Maiti, P., Hikosaka, M., Yamada, K., Toda, A., Gu, F., 2000. Lamellar thickening in isotactic polypropylene with high tacticity crystallized at high temperature. Macromolecules 33, 9069–9075.

Matsuda, H., Aoike, T., Uehara, H., Yamanobe, T., Komoto, T., 2001. Overlapping of different rearrangement mechanisms upon annealing for solution-crystallized polyethylene. Polymer 42, 5013–5021.

McLeish, T.C.B., Larson, R.G., 1998. Molecular constitutive equations for a class of branched polymers: the pom–pom polymer. Journal of Rheology 42, 81–110.

Meyer, R.W., Pruitt, L.A., 2001. The effect of cyclic true strain on the morphology, structure, and relaxation behavior of ultra high molecular weight polyethylene. Polymer 42, 5293–5306.

Monasse, B., Ferrandez, P., Delamare, F., Montmitonnet, P., Haudin, J.M., 1997. Crystallization temperature effect on the solid-state rheology of a high-density polyethylene under compression. Polymer Engineering and Science 37, 1684–1693.

Nitta, K.-H., Takayanagi, M., 1999. Role of tie molecules in the yielding deformation of isotactic polypropylene. Journal of Polymer Science. Part B: Polymer Physics 37, 357–368.

Nitta, K.-H., Takayanagi, M., 2000. Tensile yield of isotactic polypropylene in terms of a lamellar-cluster model. Journal of Polymer Science. Part B: Polymer Physics 38, 1037–1044.

Oberhauser, J.P., Leal, L.G., Mead, D.W., 1998. The response of entangled polymer solutions to step changes of shear rate: signatures of segmental stretch? Journal of Polymer Science. Part B: Polymer Physics 36, 265–280.

Osaki, K., Inoue, T., Isomura, T., 2000. Stress overshoot of polymer solutions at high rates of shear. Journal of Polymer Science. Part B: Polymer Physics 38, 1917–1925.

Powers, J.M., Caddell, R.M., 1972. The macroscopic volume changes of selected polymers subjected to uniform tensile deformation. Polymer Engineering and Science 12, 432–436.

Seguela, R., 2002. Dislocation approach to the plastic deformation of semicrystalline polymers, kinetic aspects for polyethylene and polypropylene. Journal of Polymer Science B: Polymer Physics 40, 593–601.

Seguela, R., Staniek, E., Escaig, B., Fillon, B., 1999. Plastic deformation of polypropylene in relation to crystalline structure. Journal of Applied Polymer Science 71, 1873–1885.

Sun, N., Fong, C.F., De Kee, D., 2000. A non-affine transient network model. Rheologica Acta 39, 174–179.

Sweeney, J., Collins, T.L.D., Coates, P.D., Ward, I.M., 1997. Application of an elastic model to the large deformation, high temperature stretching of polypropylene. Polymer 38, 5991–5999.

Sweeney, J., Collins, T.L.D., Coates, P.D., Duckett, R.A., 1999. High-temperature large strain viscoelastic behavior of polypropylene modelled using an inhomogeneously strained network. Journal of Applied Polymer Science 72, 563–575.

Tanaka, F., Edwards, S.F., 1992. Viscoelastic properties of physically cross-linked networks. Transient network theory. Macromolecules 25, 1516–1523.

Treloar, L.R.G., 1975. The Physics of Rubber Elasticity. Clarendon Press, Oxford.

Truesdell, C., 1977. A First Course in Rational Continuum Mechanics. Academic Press, New York.

Verma, R., Marand, H., Hsiao, B., 1996. Morphological changes during secondary crystallization and subsequent melting in poly(ether ether ketone) as studied by real time small angle X-ray scattering. Macromolecules 29, 7767–7775.

Wedgewood, L.E., Geurts, K.R., 1995. A non-affine network model for polymer melts. Rheologica Acta 34, 196–208.

Whittle, M., Dickinson, E., 1997. Stress overshoot in a model particle gel. Journal of Chemical Physics 107, 10191–10200.